R. & M. No. 3321

MINISTRY OF AVIATION

AERONAUTICAL RESEARCH COUNCIL
REPORTS AND MEMORANDA

Some Measurements of Shock-wave Attenuation in Channels of Various Cross-Sections

By L. BERNSTEIN, B.Sc. (Eng.), Ph.D.

LONDON: HER MAJESTY'S STATIONERY OFFICE
1963
PRICE 15*s.* 6*d.* NET

Some Measurements of Shock-wave Attenuation in Channels of Various Cross-Sections

By L. BERNSTEIN, B.Sc. (Eng.), Ph.D.

COMMUNICATED BY PROFESSOR A. D. YOUNG

Reports and Memoranda No. 3321†*

February, 1961

Summary.

Apparatus is described for the measurement of shock attenuation in channels of several configurations. A circular-bore channel, a square-bore channel and converging and diverging channels have been investigated. Measurements of hot-flow duration and wall pressure variations in the shock tube have also been made. It is concluded that convergence of the shock-tube channel provides an attractive method of alleviating attenuation, particularly since the hot-flow durations are not significantly altered by a slow convergence.

1. *Introduction.*

The development of the shock tube and its modifications[1] for research in high-stagnation enthalpy gas dynamics, has led to several investigations, both theoretical[2 to 5] and experimental[5 to 9], of the attenuation of shock waves in tubes. All these investigations have been confined to measuring the shock-wave trajectories in channels of uniform bore, and the majority are concerned with only relatively weak shocks. Only Refs. 6 and 7 report the results of measurements using strong shocks, and of the theoretical approaches only Ref. 4 claims to be applicable to strong shocks, though in some respects it does not agree qualitatively with experiment[22].

The present paper describes some further measurements on the attenuation of moderately strong shock waves in uniform-bore tubes, and also in tubes of slowly varying cross-section. The effects of both a convergence and a divergence have been investigated, and in all cases hydrogen was used to drive a shock wave in nitrogen.

The effects of the convergence on the duration of hot flow has been measured, and is shown to be small. On this account, it is suggested that the alleviation of attenuation by a channel convergence is an attractive proposition.

Measurements of wall static pressure have also been made using a cheap, simple, robust gauge employing a barium titanate ceramic plate as the sensing element, and these are compared with the results of Ref. 6.

The experimental results are discussed in relation to the available theories.

* The work reported here was carried out at Queen Mary College and presented as part of a thesis for the degree of Ph.D. in the University of London.

† Replaces A.R.C. 22,619.

2. *Apparatus.*

The basic apparatus consists of two shock tubes, one circular in cross-section, the other rectangular, together with timing equipment for the measurement of the shock-wave trajectories, and auxiliary instruments for determining the hot-flow duration and pressure variation behind the shock. These are briefly described in the following sub-sections. Detailed descriptions may be found in Ref. 11.

2.1. *The Shock Tubes.*

The circular-cross-section shock-tube channel is made up of several 3 ft lengths of cold-drawn stainless-steel tubing of $1\frac{1}{2}$ in. nominal bore and $\frac{1}{4}$ in. thick wall, alternating with shorter sections, 6 in. long, which carry the shock-detection instruments. These latter are of mild steel, sleeved with stainless steel to avoid corrosion, and each section has four instrument ports in each flange, thus giving a measuring arm of 4·80 in., Fig. 2. After machining to remove the drawing marks, the whole channel was assembled and honed, being finally some $16\frac{1}{2}$ ft in length and of 1·670 in. bore diameter; the steps at the junctions are less than 0·0005 in.

The high-pressure chamber consists of a 4 ft length of the same tube, unmachined so as to retain the thick wall. A 6 in. long section serves to match the two bores, and it carries a single instrument port in its downstream flange for triggering electronic apparatus shortly after diaphragm burst.

The advantage of this method of mounting the instruments is that they are easily accessible when mounted; consequently it can be ascertained that they present a minimum of disturbance to the flow.

The diaphragm, Melinex throughout these experiments, is carried in a special block, which is sandwiched between the flanges of the chamber and channel. Diaphragm bursting is accomplished by means of a simple spring-loaded plunger, axially mounted in the chamber, which is released manually by operating a pawl.

O-ring seals are used throughout, both for vacuum and pressure sealing.

The whole shock tube is mounted on a Dexion angle-iron frame, the chamber being clamped to this frame. The channel sits on rollers which run on a single rail, $2\frac{1}{2}$ in. wide on the top of the frame, thereby resulting in easy breakdown for replacing spent diaphragms.

The rectangular-bore shock tube (Fig. 3) is fabricated from bars and plates of Duralumin, in two 8 ft lengths. The side plates are 1 in. thick and sealing is effected by circular-cross-section cord seals set in dovetail grooves in the bars. In practice some Apiezon Q compound is needed under the cords, because of machining marks in the walls of the grooves. The seals are compressed by the side plates which are bolted at 2 in. intervals; dowels, to maintain accurately the bore size, and draw-off bolts are located at 4 in. intervals. The two 8 ft lengths are coupled together using a $\frac{1}{2}$ in. thick plate, with a shallow groove in each face. These grooves cover the ends of the cord seals and carry an Elastomer gasket (*see* Fig. 3). Similar plates are used at the ends.

The lower bar of one of the lengths is replaceable by one of two other bars. In its normal configuration, the bore of the tube is $1\frac{1}{2}$ in. square throughout its length. When the replacement bars are used, one of the 8 ft lengths has a tapered bore—in one case from $1\frac{1}{2}$ in. square to 1 in. × $1\frac{1}{2}$ in. and in the other case to 2 in. × $1\frac{1}{2}$ in. Accurate alignment of the bores of the two sections is accomplished by means of dowels in the ends of the bars.

The same high-pressure chamber and diaphragm blocks as are used with the circular-bore tube, are employed, a cast-steel transition section, from round to square, being used to aid shock formation.

Instrument mounting is simplified using plugs, Fig. 4, matched to orifices at 18 in. intervals in one of the side plates, so as to fit flush with the bore wall. Into these plugs are mounted the transducers—again flush with the bore wall—correctly aligned so as to be parallel with the shock front. The 6 in. section carrying the single transducer is again used immediately downstream of the diaphragm, the first measuring station being 24 in. from the diaphragm.

So as to provide a minimum of disturbance to the flow, gas inlet and outlet orifices are confined to the end plates of the shock tube, all necessary junctions being in the external pipe work. A schematic diagram of the system is shown in Fig. 5.

Valves on the low-pressure side of the equipment are modified high-pressure needle-control valves. The chamber pressure is measured by one of two 10 in. diameter gauges, covering overlapping ranges: a standard test gauge calibrated 0(5)400 p.s.i.g. and a test gauge calibrated 0(50)2500 p.s.i.g. Each gauge is duplicated by a smaller one for checking purposes.

The channel pressure is measured using one of three gauges: a mercury manometer; a barometrically compensated Edwards' dial gauge 0–40 mm Hg; and a Pirani vacuum gauge for the range 0·001–10 mm Hg.

A two-stage rotary vacuum pump—Edwards' Speedivac 2SC450A—is used to exhaust the channel; with the numerous junctions in the system, the ultimate vacuums in the systems were about 0·5 mm Hg for the circular-bore channel and about 0·1 mm Hg for the rectangular-bore tube. A single-stage pump is used to exhaust the chamber prior to charging with hydrogen, a dial gauge calibrated 0–100 mm Hg monitoring this evacuation.

2.2. *The Timing Equipment.*

In order to measure the shock trajectory along the tube for each run, a single long-duration, high-resolution time-base has been employed, this being considered the cheapest method. Of the many versions possible, the spiral display was chosen as being the most accurate, no time losses being incurred due to beam 'turn-round' such as are inherent in raster displays. A C.R.O. tube with a central electrode was available, so that calibration signals and shock-passage signals could be displayed radially.

Such a time-base is essentially an analogue device whereby time is displayed as length. The shortest measuring arm in the shock tubes is 0·4 ft in a total channel length of about $16\frac{1}{2}$ ft. Thus if the time interval over this arm is to be measured within 1%, the overall time-base resolution must be better than 0·03%. This is possible with about 10 'circles' on a 5 in. diameter C.R.O. face.

The basic time-base waveforms are generated by the circuit of Fig. 6, in which four decaying sine waves successively phase-shifted by 90°, are generated at A, B, C and D upon receipt of a square trigger-pulse at G. The frequency, or time/circle is controlled by R_2 and R_3 which are mechanically coupled. These waveforms are amplified and fed to the deflection plates of the C.R.O. With a number of interrelated circuits, shown schematically in Fig. 7, a decaying spiral is produced on the screen, the trace brightening-pulse being controlled to operate when the spiral has properly formed.

As the spiral cannot be relied upon to be equi-angular, calibration pulses at 10 microsecond intervals are provided by a Schmitt trigger circuit used as an oscillator[12]. Synchronisation pulses are provided from a Furzehill portable frequency standard. This calibration signal is fed to the tube coating.

A single counter chronometer, with a resolution of $\pm\frac{1}{8}$ microsecond—manufactured by Rank-Cintel Ltd.—was also available for single time-interval measurements.

2.3. *The Shock-Passage Detectors.*

Barium titanate ceramics were used to detect the pressure change upon shock passage. They were chosen for their reliability and robustness, and because they could be used over a wide range of conditions. They have the added advantage that they are easily machined, and can be mounted flush with the tube wall. In the present investigation, ceramic plates, 0·020 in. × 0·5 in. × 0·25 in., polarised across the major faces, were used. They are mounted in a Tufnol plug, Fig. 4, so that the plate is parallel to the shock front, the leads being soldered inside copper pins which fit a standard twin-lead, screened-cable socket. These Tufnol plugs fit into the orifices of the 6 in. sections (Fig. 2) and into the instrument plugs of the rectangular-bore channel. In each case they are easily machined flush with the bore wall. The response time of these ceramics was unfortunately rather long—about 6 microseconds. The employment of much shorter plates (shorter that is, in the direction perpendicular to the tube axis) considerably reduces this rise-time. Plate I illustrates the improvement, trace (a) being the 0·5 in. long plate, and trace (b) the output of a plate about $\frac{1}{8}$ in. long, in which the rise-time is reduced to about one microsecond. However in all the results reported here, the larger plates were used, and the errors were calibrated as described in Section 3.2.

Before being fed to the counter or oscillograph time-base, the transducer output was amplified and shaped by the conventional trigger-amplifier of Fig. 8. Positive and negative pulses of 60 volts amplitude are available from each unit, and since the C.R.O. and counter required positive triggering pulses, the negative pulses were fed to the central electrode of the time-base tube. The crystal diodes were introduced to prevent dissipation of the pulses in the parallel output impedances of all the other units which are connected to the common C.R.O. input terminal.

The thyratron grid bias was set to an arbitrary standard of -10 volts. The switched attenuator at the input was provided to discriminate against spurious signals due to mechanical vibration of the tube. This latter was occasionally troublesome in the circular-bore tube, where it was not found possible to completely isolate the transducers, as it was in the rectangular cross-section tube. For this reason, experiments on the former channel are not so comprehensive as on the others. The mechanical vibrations appeared to be some kind of 'barrel' mode, advancing at shock velocity, and partial isolation was achieved by using 'soft', O-ring mountings, and allowing no rigid surfaces to make contact.

2.4. *The Pressure Transducers.*

The successful development of the barium titanate ceramic plates as shock-passage detectors, led to the possibility of their being used as pressure transducers. Using the cathode-follower amplifier* of Fig. 9 as a buffer stage between the C.R.O. and the relatively high impedance ceramic (about 40 megohms in parallel with 1000 pf), the traces shown in Plate I, (c) and (d), were obtained. It can be seen from these traces that shortly after shock passage, a fairly large negative excursion of the signal took place, the delay depending on the shock strength. The possibility of this resulting from gas leakage around the sides of the Tufnol plug, and thereby producing a hydrostatic response (which is of opposite sign) was eliminated by sealing the potential gap with Scotch tape. In so doing it was noted that by placing Scotch tape over the exposed end of the ceramic, the effect

* V1 is a carefully selected valve as regards grid-current characteristics. That portion of the circuit containing the relay was provided only to measure the input impedance of the cathode-follower—the relay was removed for normal operation.

was eliminated, and its use was therefore standardised. Typical traces are shown in Plate I (e), (f) and Plate II (a), (b), (c), trace I (e) being without the cathode-follower amplifier.

The negative excursion was probably due to short-circuiting of the ceramic by incandescent dust in the tube—it took place when temperatures behind the shock wave were far below those at which an appreciable number of electrons were likely to be present as a result of nitrogen ionization. The small change in surface temperature of the ceramic is unlikely to have so marked an effect.

The problem of insulating the transducers from stray mechanical vibration has already been mentioned. There is however, an inherent vibration of the transducer and its mount, when a shock load is applied. This 'ringing' is apparent in Plates I and II, and although it is only of moderate amplitude compared with the main signal at high channel pressures, it is troublesome at low values. It has not been possible to eliminate this ringing. One interesting approach is suggested by Edwards[13], but was considered impractical in the present circumstances. His method is to back the ceramic by a long bar of the same acoustic impedance, so that the reflected pulse is delayed by a time proportional to the total length of the system. However, complete elimination of the ringing during the time intervals of interest, would require inordinately long bars. One approach may be to employ an acoustically matched anvil with a high dissipation factor, so that the reflected pulse is very weak.

2.5. *Interface-Passage Detectors.*

Thin-film thermometer gauges[15, 16] were used to detect the passage of the interface. The platinum film was painted and then fired onto a short length of Pyrex rod so as to form the front stagnation line of a cylinder which was glued with Araldite into a Tufnol plug similar to those used for the ceramics (*see* Fig. 10). The rod projected about half an inch into the flow. Probes made in this way had a cold resistance of 50–100 ohms and this increased very slowly, run by run. Provided they were not hit by pieces of diaphragm, they lasted for many runs. They could not however be used with high pressures in the tube, since the glass was not able to withstand the high shock loading. Since however, a wide variety of shock strengths could be investigated even with this restriction, no attempts were made to improve the design, though a simple backing support should prove adequate.

These resistance thermometers were operated at a constant current of about 10 mA, the signal being amplified by a factor of about 10 before being fed to the oscilloscope *via* a cathode-follower output stage.

3. *Experimental Procedure and Discussion of Results.*

Throughout these experiments, high-pressure hydrogen was used to drive a shock wave in nitrogen. Although a high degree of gas purity was not required *per se*, the safety procedure adopted in charging the shock tubes led to fairly pure gas samples. This procedure was designed to prevent contamination of the laboratory with hydrogen, and it also ensured that the chamber and channel were each free of that gas which should occupy the other. The nitrogen used was specifically free of oxygen.

The calibration procedures are described in the following sections, it being convenient to consider the mechanical apparatus, the electronic timing equipment and the pressure transducers, separately.

3.1. *Calibration of Mechanical Measuring Equipment.*

It is well known that the strength of the shock generated in the shock tube is dependent upon the

pressure ratio across the diaphragm. The relation between this pressure ratio (P_{41}) and the shock Mach number (M_s) is, for the case of ideal gases (*see* Ref. 17, for example),

$$P_{41} = \frac{1}{\alpha_1}\left\{\frac{M_s^2}{\beta_1} - 1\right\}\left\{1 - \frac{\gamma_4 - 1}{\gamma_1 + 1} A_{14}\left(M_s - \frac{1}{M_s}\right)\right\}^{-1/\beta_4} \tag{3.1}$$

where

$$A_{14} = \frac{a_1}{a_4}$$

is the sound speed ratio of the two gases initially on either side of the diaphragm (Fig. 1)

$$\alpha = \frac{\gamma + 1}{\gamma - 1} \text{ and } \beta = \frac{\gamma - 1}{2\gamma}$$

where γ is the specific-heat ratio and the suffices refer to the regions so labelled in Fig. 1.
By differentiating equation (3.1), we find

$$\frac{dM_s}{M_s} = \frac{1}{f(M_s)} \frac{dP_{41}}{P_{41}} \tag{3.2}$$

where

$$f(M_s) = \frac{2M^2_s}{M^2_s - \beta_1} + \frac{M_s + \dfrac{1}{M_s}}{\beta_4\left[\alpha_1\sqrt{(B_{14}E_{41})} - \left(M_s - \dfrac{1}{M_s}\right)\right]} \tag{3.3}$$

$$B_{14} = \frac{\beta_1}{\beta_4} \text{ and } E_{41} = \frac{(C_v T)_4}{(C_v T)_1} \text{ the internal-energy ratio.}$$

Now $1/f$ has a maximum value of about $0{\cdot}35$ for a H_2/N_2 shock tube at a shock Mach number, $M_s \approx 1\frac{1}{2}$, while for most of the range of interest, it is less than $0{\cdot}3$. Thus a 4% error in P_{41} results in a maximum error of $1{\cdot}3\%$ in the shock speed, a smaller discrepancy than that produced by variable diaphragm characteristics (*see* Section 3.4). In any event repeatability was the primary requirement, and this could be achieved without calibrating the pressure gauges.

The vacuum gauges did not agree (within 1 mm Hg), in their overlapping ranges, and neither did the chamber pressure gauges, but that these errors are insignificant is borne out by the maximum shock strengths obtained for a given diaphragm pressure ratio, but varying channel pressures.

The variations in the bursting pressures, of diaphragms of a particular thickness, place a severe restriction on the repeatability of a given set of initial conditions if pressure alone is to cause rupture. Mechanical bursting was therefore employed, the diaphragms being chosen such that their natural bursting pressure did not exceed by more than 10% the pressure at which rupture was to be precipitated.

3.2. *Calibration of Electronic Timing Equipment.*

The relation between the output pulse of the thyratron in the amplifier-trigger units, which ultimately provides the timing signal, and the shock's passage of a given station is clearly dependent upon the rise-time of the transducer at that station, and the characteristics of the associated amplifier. With a finite rise-time to the transducer signal, the exact instant of 'firing' of the thyratron will depend upon the slope of the amplified signal that appears at the control grid of this valve, and also on its 'breakdown' voltage. It is therefore necessary to calibrate the delay in each system—transducer plus amplifier—arising from the long transducer rise-time.

An artificial pulse simulating the transducer output was fed to the input terminals of two of the amplifier-trigger units, and the output pulses were fed to the START and STOP gates of the Cintel 8 Mc/sec counter chronometer. The relative delay was noted for a range of input amplitudes up to 100 mV with the attenuator in position 1 (Fig. 8). This was repeated for all the units, using one as an arbitrary standard, and maintaining a fixed bias of -10 volts on the thyratron grids. The input-output voltage characteristics of all the amplifiers and their attenuators were then measured using an oscilloscope.

Using this data and the transducer sensitivity (*see* Section 3.3), the correction for any set of conditions could then be calculated. A typical set of corrections is shown in Fig. 11 where it is apparent that they nowhere exceed one microsecond. It was found convenient to pair the units, so that corrections could be made to successive time intervals along the tube. The output signals are displayed on the spiral time-base (Plate III), which also carries a calibration signal. This time-base is recorded using Kodak Royal-X Pan film in a $2\frac{1}{4}$ in. square format. Time intervals are obtained using an enlarger and a transparent radial grid to aid interpolation.

During each run, the overall time between the shock's passage of the first and last stations was recorded using the Cintel chronometer, and this always agreed with that measured on the spiral to within one microsecond. The Furzehill portable frequency standard, and the 8 Mc/sec crystal oscillator in the chronometer had previously been checked against the standard frequency of 200 kc/sec broadcast by the B.B.C. from Droitwich.

3.3. *Calibration of Pressure Transducers.*

Attempts to calibrate the pressure transducers independently of the shock tube were not very successful. The method tried was to mount the ceramic in a chamber containing oil at a known pressure, and then to release this pressure suddenly by bursting a diaphragm. Considerable scatter and day-to-day variation were observed.

The second method used involved the shock tube. By employing a series of equal-strength shocks travelling into gas at different, known pressures, the output signal was measured as a function of the calculated pressure rise. Fairly good linearity was observed, but there was still considerable day-to-day variation (the ceramics are sensitive to temperature and humidity). On the whole, runs made in a single day showed more consistency than those over a longer period. Fig. 12 shows data for several nominally identical ceramics obtained over a wide range of conditions—both channel pressure and shock strength were varied. Some of the scatter is undoubtedly due to inconsistencies in the measurements of initial channel pressures—it will be recalled that the gauges did not agree in their overlapping regions.

The majority of the points, obtained with a single transducer at 112 tube widths from the diaphragm, suggest that with development, these transducers may provide a cheap, simple way of measuring pressure.

In the meantime, these results may be taken to imply that for any one run, the output signal is proportional to the pressure, the calibration factor being supplied by the initial step due to the shock passage.

The sensitivity is considerably greater than that quoted by the manufacturer, which is about 0·33 mV per mm Hg for a plate 0·020 in. thick subject to a pressure load perpendicular to the axis of polarisation.

3.4. *Effects of Variable Diaphragm Bursting.*

Because of their unreliable bursting characteristics in a small, circular orifice, metal diaphragms were not used in the present investigations. A few tests were made in the circular-bore tube to discover the effects on the shock trajectory of a 'bad' burst, and of mechanical as distinct from natural bursting. Fig. 13 shows the results of too thick a diaphragm being used, so that it split rather than petalled. The bad burst is characterised by a long, slow acceleration of the shock to its maximum velocity over about 40 tube diameters. In Fig. 14 are plotted the results for natural and mechanical bursts at approximately the same initial conditions. The dotted curves represent the natural bursts, and it can be seen that the differences between these nominally identical runs and those obtained using the plunger are of the same order. The scatter of points for each run is due to the different length measuring arms (*see* Section 3.8).

This uncontrollable scatter made any direct comparison of individual runs under different initial conditions, somewhat meaningless. The significance of the arithmetic mean trajectory for several runs at the same initial conditions is uncertain, in view of the different trajectories sometimes produced. However, the practice adopted was that several runs were made at each set of conditions, and the mean trajectory was used to represent a typical one for these conditions—any unusual curves were omitted from the averaging process. A typical set of such runs is shown in Fig. 15. The results presented in the following section are, in general, the average trajectories of at least four runs; the chief exceptions are those for the diverging channel, where for the most part only three runs were made. The initial conditions and the number of runs averaged are summarised in Table 1.

3.5. *The Attenuation of Shock Waves in Channels of Various Cross-sections.*

The experimental procedure described in the preceding sections, was applied to obtain a series of shock trajectories along the various channel configurations. Throughout these experiments, hydrogen was used to drive a shock in nitrogen. The experiments were designed to determine:

(i) The importance of cross-sectional configuration, for channels of approximately the same hydraulic diameter;

(ii) The effect of channel pressure—i.e., of Reynolds number—on the attenuation of shock waves produced by a fixed value of diaphragm pressure ratio; and

(iii) The effects of tapering a section of the channel, with a view to the alleviation of this attenuation by converging the bore.

So far as the writer is aware, there has not been published to date, any experimental justification of the assumption in unsteady flow, that channels of similar hydraulic diameter, irrespective of cross-sectional shape, will exhibit similar overall characteristics. Previous investigators[5, 6, 7] have confined their experiments to single channels, while the experiments of Emrich and Curtis[18] were carried out in tubes of widely different hydraulic diameter. The present results provide some justification of the above assumption. A direct comparison of the results in the circular-bore channel ($d = 1{\cdot}670$ in.) and the square-bore channel ($d = 1{\cdot}5$ in.) is presented in Figs. 16a to c.

Even the unusual features of the shock trajectories are reproduced in the two channels—*see* Fig. 16c. The flattening of the trajectory some distance from the diaphragm is probably a characteristic of the latter's bursting imperfections. In this case a compound diaphragm of four thicknesses was used, and a slow opening is quite common in these circumstances. A similar tendency is discernible

in Fig. 16a; here a single thickness was used, whose natural bursting pressure could be slightly more than 10% above that at which rupture was precipitated—in such a marginal case no advantage was to be gained by using a compound diaphragm which was likely to exhibit similar behaviour.

The effects of Reynolds number on the shock-wave attenuation are more difficult to discern. Tests were made at a number of diaphragm pressure ratios, at each of which the channel pressure was varied. The results of these runs, carried out on both the circular- and square-cross-section channels are illustrated in Fig. 17a, b and Fig. 18a to e, respectively. The most comprehensive set of runs was carried out in the square-bore tube, but they cover a wide Reynolds number range only at a fairly low shock Mach number. Because of pressure limitations, the range of Reynolds numbers at high shock Mach numbers was restricted (these restrictions arose from a lack of suitable diaphragm materials, the chamber being designed to operate at pressures up to 2000 p.s.i.).

Shock trajectories were also obtained for roughly the same range of initial conditions (*see* Table 1) for both the converging and diverging channels. The results are presented in Figs. 19a to c where they are compared with those for the uniform-bore channel. It will be recalled that only the last 8 ft of channel is tapered, so that a discontinuity appears (at $x/h = 74$). The tube width, h, is assumed constant at 1·500 in. for all cases.

It is clear that in the tubes investigated, Reynolds number is of little importance, except perhaps for channel pressures below about 5 mm Hg. (The large scale of the plots should be noted.) This is in agreement with the results of Jones[6] who also discovered no effects, and with those of Duff[8] who found a marked dependence for low channel pressures of the order of 1 mm Hg.

The theoretical predictions of Refs. 3 to 5 all indicate a Reynolds number dependence, and their curves of shock-velocity attenuation are all concave upwards. The present results show no consistent tendency, but are mainly concave downwards. One would expect that as the shock wave weakened, the attenuation would correspondingly diminish—that is, the curves should be concave upwards. One is forced to draw the conclusion that the diaphragm rupturing characteristics, dominate the shock trajectory for most of the tube length investigated here.

Certainly the only theory applicable to strong shocks, that due to Spence and Woods[4] predicts the wrong order of shock-velocity decrement. Their calculations are all for shocks driven in air, initially at 0·05 atmospheres; however some comparison may be made.

For a shock, of initial Mach number 8, driven by hydrogen, they predict a fall to $M_s = 6{\cdot}8$ at 120 tube diameters from the diaphragm, assuming a turbulent boundary layer. The experimental results of Fig. 16a show considerably less attenuation than this for a much lower Reynolds number—channel pressure of 2 mm Hg. Their theoretical result is

$$M_s = M_{s0}\left\{1 - CK\left(\frac{u_2 x}{\nu_m}\right)^{m-1}\left(\frac{x}{d}\right)\right\} \tag{3.4}$$

where

M_s is the shock Mach number, suffix $_0$ indicating the initial value;

C, K and m are parameters depending on the gases used, the shock strength and the boundary-layer structure;

x is the distance from the diaphragm;

u_2 is the gas velocity behind the shock wave; and

$\nu_m = \dfrac{\mu_m}{\rho_m}$ is the kinematic viscosity evaluated at the mean enthalpy.

Now μ_m depends only on the temperature behind the shock wave, which for a given set of initial conditions is a function only of shock strength (neglecting real-gas effects). Thus we should expect the shock-velocity decrement to be proportional to ${\rho_m}^{m-1}$, that is to ${p_1}^{m-1}$ for a particular shock strength. Since $m = \frac{1}{2}$ for the laminar boundary layer, and $m = 4/5$ for the turbulent layer, there should be more attenuation for the experimental case at $p_1 = 2$ mm Hg, than Spence and Woods predict for $p_1 = 38$ mm Hg (0·05 atmos.), which is clearly not so.

There are of course factors which are ignored in all the theories. The cold flow behind the interface is highly turbulent having passed over the remains of the diaphragm, and disturbances may perhaps be transmitted downstream. The interface stability is another factor which may considerably affect the shock motion. Furthermore, viewed from the shock, the interface is considerably closer than is predicted by ideal theory (*see* Section 3.6) and in consequence, upstream-travelling disturbances generated in the hot-flow region are likely to arrive at the shock after reflection at the interface, much sooner than is predicted by theories which take no account of this interface acceleration. Correspondingly waves generated in the cold region behind the interface, will take longer to overtake the shock.

It seems therefore, in view of the complex and at present largely indeterminate nature of the factors causing it, that the attenuation of shock waves in pipes is not described by the available theories with sufficient accuracy for quantitative predictions.

The difficulty of accounting for the behaviour of the shock wave in the uniform channel is increased when a taper is introduced. The available theoretical models[19, 20] are all concerned with inviscid flows. However with a knowledge of the attenuation in the uniform tubes, it is possible to 'correct' the measured trajectories by adding the decrement due to viscous forces and heat conduction. Essentially, the theory of Chisnell[20] predicts that

$$A = Q \exp\left\{ - \int \frac{2M_s dM_s}{({M^2}_s - 1)K(M_s)} \right\} \tag{3.5}$$

where

A is the cross-sectional area of the tube,

Q is a constant depending on the initial conditions

and

$K(M_s)$ is a slowly varying function of shock Mach number, M_s, being 0·5 at $M_s = 1$ and 0·394 at $M_s = \infty$ for $\gamma = 7/5$.

For strong shocks ($M_s \geqslant 5$), we may assume $K \doteq 0{\cdot}4$ in which case equation (3.5) may be integrated to give

$$\left[\frac{A}{A_0}\right]^{0{\cdot}4} = \frac{{M_s}_0{}^2 - 1}{M_s{}^2 - 1} \tag{3.6}$$

where suffix $_0$ indicates the conditions at entry to the taper.

Fig. 20 shows a number of the 'corrected' experimental trajectories compared with this equation. The corrections are simply taken as the Mach number decrement suffered by the shocks in the uniform tube at the same initial conditions. When it is recalled that the mean hydraulic diameter of the converging tube is smaller than that of the uniform tube, so that the viscous attenuation has been underestimated, the agreement is satisfactory. A similar argument may be used to account for the

discrepancy of opposite sign in the case of the diverging channel. However, an attempt to correct the curves for the different hydraulic diameters, based on equation (3.4) leads to a slight improvement, but not a significant one.

3.6. *Measurements of Steady-Flow Duration.*

Using the thin-film-thermometer probes, records of the hot-flow duration were obtained in the uniform and converging rectangular-bore channels at a particular station ($x/h = 112$). Typical traces are shown in Plate II. The records differ according to shock strength—weak shocks, trace (d), give rise to a parabolic voltage-time signal followed by fluctuations in the trace at C. For stronger shocks, trace (e), the arrival of the interface at **C**, is considerably more pronounced. This latter is to be expected, since theoretically there is a discontinuity in recovery temperature at the interface. As the flow proceeds away from the diaphragm, the sharp discontinuity at the interface spreads.[9] For weak shocks, the smaller discontinuity is probably spread more rapidly.

The steady-flow durations, as measured from these records, are shown in Figs. 21 and 22 for the two channels, the abscissae being the local shock Mach number. Significant Reynolds number effects are noticeable for low initial channel pressures, in accordance with the results of Duff[8].

No significant difference is found between the two channels, the empirical curves on Fig. 22 being those for the uniform-bore channel.

The experimental results fall markedly below the theoretical curve for an ideal, imperfect gas. Other investigators (*see*, for example, Ref. 14) have also noted this. At a comparable number of tube diameters from the diaphragm (124), Henshall[14] reports about the same fraction of the theoretical running time. By a theoretical approach, Anderson[21] suggests that the conflicting effects of the receding interface, as viewed from the shock, and of viscous action, lead to a maximum running time for each tube and set of initial conditions. This is brought about by the loss of test gas within the boundary layer to the region behind the interface, the rate of this entrainment being eventually equal to that being generated by the differential velocities of the shock and interface. Although neither Henshall's data nor that of the present investigation are sufficiently comprehensive to establish this theory, they certainly go some way towards supporting it.

In an attempt to detect the presence of secondary waves formed by the interaction of the shock and the convergence, a few runs were made with weak shocks. Plate II(f) illustrates the arrival of these secondary waves at a station 4·75 ft from the beginning of the convergence for a shock Mach number of 2·13. A detailed study of these waves was outside the scope of the present investigation, in which it was only necessary to ascertain that these secondary waves did not prematurely terminate the steady-flow region. No such waves were detected for the range of shock strengths plotted in Fig. 22.

The severe reduction in the extent of uniform flow below the theoretical value, makes the region immediately behind the shock front in which relaxation effects occur, of greater importance. The extent of uniform flow is reduced at 'both ends'. Furthermore due to imperfections in the diaphragm bursting process, and shock attenuation, the actual shock Mach number attained for a given diaphragm pressure ratio is less at a particular station than that predicted theoretically. Consequently, in order to realise a particular shock Mach number at the working section of the tube, the maximum undisturbed channel pressure will be lower than the ideal value, for a fixed chamber pressure (usually limited by structural considerations). The relaxation region will correspondingly be larger. Convergence of the channel would therefore seem a useful way of maintaining the shock strength,

and thereby reducing the extent of the non-uniform region, particularly since a slow convergence appears not to affect the running time.

3.7. *Wall Pressure Measurements.*

Using the apparatus previously described, pressure records were obtained over a wide range of initial conditions. Typical traces are shown in Plates I(f) and II(a), (b), (c). In spite of the troublesome ringing at low initial channel pressures, it is clear that these records are characterised by a steady-pressure region, followed by one of steep gradient. Records taken using a longer-duration time-base show a subsequent fall in the pressure which may be correlated with the arrival of the reflected head of the rarefaction wave generated at diaphragm burst. The records can therefore be analysed with some confidence.

Similar records were obtained by Jones[6], who found that the duration of steady pressure varied with distance from the diaphragm, shock strength, and initial channel pressure.

Fig. 23a shows the variation of steady-pressure duration as measured in the $1\frac{1}{2}$ in. square-bore channel for a particular set of initial conditions—the local shock Mach number varies due to attenuation. The duration of hot flow at these conditions, measured on a single run at $x/h = 112$, falls slightly below this curve.

Fig. 23b shows the variation in the extent of this steady-pressure region as a function of channel pressure for a fixed diaphragm pressure ratio at the station $x/h = 112$. At low channel pressures, the excessive ringing precluded accurate measurements, but the trend is clear.

Theoretical considerations[22] suggest that the region of pressure gradient following that of constant pressure might arise as the boundary layer suffers transition from laminar to turbulent flow. It is however, not obvious how the relevant Reynolds number describing the 'transition point' is to be determined. One suggestion involves the distance travelled by a particle before it reaches the transition point, together with the fluid properties of the mainstream outside the boundary layer. Another, on analogy with the steady flow relative to the shock (with the moving wall as a boundary condition) uses the distance from the shock to the transition point. If l is the relevant distance, we may write

$$R_T = \frac{u_2 \rho_2 l}{\mu_2} \tag{3.7}$$

where suffix $_2$ refers to the hot region (Fig. 1) and the symbols have their usual meaning (*see* Notation).

In terms of the measured steady-flow duration, Δt, this becomes

$$R_T = \frac{u_2 \rho_2}{\mu_2} \Delta t \, g(M_s) \tag{3.8}$$

where $g(M_s)$ is a function of shock Mach number only, the particular function depending on which distance l is chosen as the relevant one.

Written in terms of the initial channel conditions

$$\begin{aligned} R_T &= \frac{U_{21} \Gamma_{21}}{\mu_{21}} \frac{a_1 \rho_1}{\mu_1} g(M_s) \, \Delta t \\ &= \text{constant} \times p_1 \times G(M_s) \, \Delta t \end{aligned} \tag{3.9}$$

for a constant value of T_1.

For a constant value of the shock strength, the wall-to-free-stream temperature ratio is constant (ignoring real-gas effects). Under these conditions, one would expect the transition Reynolds number to remain constant as the channel pressure was varied. Fig. 24 shows the variation of R_T with channel pressure, p_1, for a shock Mach number, $M_s \approx 4{\cdot}4$ (these points are denoted by crosses). The distance l has been taken as that travelled by a particle before it reaches the pressure gradient, *viz.*,

$$l = a_1 M_s(\Gamma_{21} - 1)\Delta t. \tag{3.10}$$

R_T is seen to be by no means constant.

Also plotted on the same axes are some points at the same shock Mach number, using the steady-flow duration as measured with the stagnation-line thermometer, which it will be recalled projected well out into the stream. In this connection it may be noted that Jones[6] inferred the arrival of the interface from a second signal emitted from his ionization probes. His results indicate considerably longer hot-flow durations than regions of steady pressure. Recalling, however, that his probes are probably close to the wall, a glance at Fig. 1 will show how the interface should arrive much later at a point near the wall, due to retardation within the boundary layer.

We are thus led to infer that transition to turbulence is precipitated by the arrival of the highly turbulent cold flow, rather than by instability of the boundary layer to small disturbances amplified within it, and that laminar flow is maintained within the hot region by the high cooling rates: $T_w/T_2 = 0{\cdot}22$ for $M_s = 4{\cdot}4$. Such a conclusion is not borne out by the overall shock-attenuation measurements, since for a laminar boundary layer, one would expect far more dependence on Reynolds number than is observed. The theory of Ref. 22, which is concerned with evaluating the pressure gradient generated by the growth of the boundary layer behind a shock wave travelling in a pipe, is somewhat tentative. Although the results suggest that a much stronger pressure gradient is generated by the growing turbulent boundary layer than by a laminar one, no account is taken of this pressure gradient in formulating the skin-friction law in the turbulent case. It is argued there, that the inclusion of a term which takes account of this interaction, will so modify the results as to reduce the differences in the effects of the growing laminar and turbulent boundary layers.

The data for other shock strengths have also been plotted on Fig. 24, points involving the steady-pressure duration and the extent of the hot flow being shown. The empirical relation between R_T and p_1 remains unexplained.

3.8. *Estimation of Experimental Errors.*

(i) *Gas purity*: As has been pointed out, a high degree of gas purity was not required, but the procedure adopted led to the following approximate *maximum* values of impurity:

Nitrogen $0{\cdot}01\%$

Hydrogen $0{\cdot}1\%$

(ii) *Diaphragm pressure ratio*: Due to gauge inaccuracies and small leaks, the diaphragm pressure ratio was not repeatable to within about $\pm 4\%$. The accuracy of the absolute value is unknown, since no gauge calibrations were performed.

(iii) *Shock-velocity measurements*: Due to inaccuracies in the time-interval measurements arising from several sources, the individual shock-velocity measurements will be in error. Most of the errors, arising from transducer response, time-base interpolations, etc., are absolute time errors. Thus the accuracy of the shock-velocity measurements will depend upon the total time interval,

that is, upon the length of the measuring arm (the error involved in measuring the latter is negligible). A further error is introduced in the case of the circular-bore tube, by the mechanical vibration before the shock arrival (this amounts to about $\pm 0{\cdot}3$ microseconds).

The *maximum* probable errors (associated with the strongest shocks) are:

Circular-bore channel:	4·8 in. measuring arm:	$< 3{\cdot}5\%$
	36 in. measuring arm:	$< 0{\cdot}5\%$
Rectangular-bore channel:	18 in. measuring arm:	$< 1\%$.

(iv) *The running-time measurements*: The main error arises from reading the oscillograph traces. This is about $\pm 1\frac{1}{2}\%$.

Concluding Remarks.

Apparatus has been developed for the measurement of shock-wave attenuation, hot-flow duration, and pressure variation within the shock tube. It is shown that barium titanate ceramic plates provide a reliable, convenient and robust method of detecting the shock passage under a wide range of conditions, provided care is taken to prevent response to mechanical vibration transmitted along the shock-tube walls.

For tubes of similar hydraulic diameter, the shape of the cross-section has been shown to be unimportant for the present class of unsteady flows, in so far as overall effects are concerned.

The effects of taper—both convergent and divergent—on the shock trajectory have been examined. These effects are as expected; convergence decreases and divergence increases the shock-velocity attenuation. By 'correcting' the trajectories in the tapered tubes for viscous attenuation, they are shown to be in fair agreement with an inviscid theory due to Chisnell[20].

A comprehensive study in a square cross-section channel has failed to reveal any significant Reynolds number effects on shock-wave attenuation, except perhaps below channel pressures of about 5 mm Hg. This is in agreement with the experimental results of Jones[6] and Duff[8], but disagrees with all theoretical predictions[2 to 5]. The experimental results are also in quantitative disagreement with the available theories. Over the channel lengths investigated, about 120 tube diameters, the diaphragm bursting process seems to influence much of the flow.

The hot-flow durations have been measured at a single station in both the uniform-bore square channel and in the converging channel. They are found to be considerably less than the theoretical values predicted for an ideal, imperfect gas, but do not differ significantly from each other. Again a Reynolds number dependence is discernible only below channel pressures of about 5 mm Hg. This is possibly due to a more extensive laminar-boundary-layer region at the lower Reynolds numbers. It is suggested, on the basis of these results, that convergence of the channel is an attractive method of alleviating the shock attenuation.

Such a method, it is argued, will reduce the extent of the non-uniform region behind the shock in which relaxation processes take place. This is important if testing is done in the simple shock tube, but of doubtful importance when the shock tube is modified by the addition of a nozzle for operation as a reflected-shock hypersonic tunnel[1]. In the latter, the gas may or may not remain in equilibrium on expanding through the nozzle, so that the advantage of the gas being in thermodynamic equilibrium at the nozzle entrance is questionable. Most of the thermal energy is, in any case, converted to kinetic energy in the nozzle.

Any pressure gradients generated in the flow by the action of boundary-layer growth have not proved detectable in the hot region, as terminated by the measured arrival of the cold front in the mainstream. A steep pressure gradient does, however, begin in the vicinity of the interface. It is tempting to infer that transition to turbulence within the boundary layer is precipitated by the arrival of the highly turbulent cold flow, but this conclusion must be treated with great caution. It is not borne out by overall shock-attenuation measurements, and the theory upon which the argument is based[22], is tentative in the extreme.

Acknowledgements.

The author would like to express his gratitude to Dr. L. G. Whitehead for his many helpful suggestions, particularly with regard to the design of the time-base. Thanks are also due to Mr. W. Montague who built much of the apparatus, and whose patience with the vacuum system was invaluable. Finally, the author would like to thank Professor A. D. Young for his encouragement during the preparation of this paper.

NOTATION

a		Speed of sound
A_{ij}		Speed-of-sound ratio a_i/a_j
B_{ij}	$=$	β_i/β_j
C_p, C_v		Specific heats at constant pressure and constant volume respectively
d		Tube diameter
h		Tube width
l		Characteristic length
M_s		Shock Mach number
p		Pressure
P_{ij}		Pressure ratio p_i/p_j
R_T		'Transition' Reynolds number
t		Time
T		Temperature
u		Gas velocity in x-direction
U_{ij}		Velocity ratio u_i/a_j
w_1		Shock-wave velocity
x		Distance from diaphragm
α	$=$	$(\gamma+1)/(\gamma-1)$
β	$=$	$(\gamma-1)/2\gamma$
γ		Specific-heat ratio C_p/C_v
Γ_{ij}		Density ratio ρ_i/ρ_j
μ		Dynamic viscosity
ν		Kinematic viscosity
ρ		Density

Suffices

0	Indicates initial value
1, 2, 3, 4	Refers to quantities in regions so labelled in Fig. 1
w	Value at the wall
m	Quantity evaluated at mean enthalpy (*see* Ref. 4).

REFERENCES

No.	*Author(s)*	*Title, etc.*
1	A. Herzberg, W. E. Smith, H. S. Glick and W. Squire	Modifications of the shock tube for the generation of hypersonic flow. Cornell Aero. Lab. Rep. AD–789–A–2. 1955.
2	R. N. Hollyer, Jr.	Attenuation in the shock tube. I. Laminar flow. *J. App. Phys.* Vol. 27. No. 3. p. 254. 1956.
3	H. Mirels	Attenuation in the shock tube due to unsteady-boundary-layer action. N.A.C.A. Report 1333. 1957.
4	D. A. Spence and B. A. Woods..	Boundary layer and combustion effects in shock-tube flows. Paper delivered at Colston Symposium, Bristol, 1959. Published by Butterworths (1960) in *Hypersonic Flow* edited by A. R. Collar and J. Tinkler.
5	R. L. Trimpi and N. B. Cohen ..	A theory for predicting the flow of real gases in shock tubes with experimental verification. N.A.C.A. Tech. Note 3375. March, 1955.
6	J. J. Jones	Experimental investigation of the attenuation of shock waves in a shock tube with hydrogen and helium as driver gases. N.A.C.A. Tech. Note 4072. July, 1957.
7	C. E. Witliff and M. R. Wilson ..	Shock-tube driver techniques and attenuation measurements. Cornell Aero. Lab. Rep. AD–1052–A–4. 1957.
8	R. E. Duff	Shock-tube performance at low initial pressure. *Phys. of Fluids.* Vol. 2. No. 2 p. 207. 1959.
9	R. J. Emrich and D. B. Wheeler	Wall effects in shock-tube flow. *Phys. of Fluids.* Vol. 1. No. 1. p. 14 to 23. 1958.
10	H. Mirels and W. H. Braun ..	Nonuniformities in shock-tube flow due to unsteady-boundary-layer action. N.A.C.A. Tech. Note 4021. May, 1957.
11	L. Bernstein	An investigation into high-speed gas flows in shock tubes. Ph.D. Thesis, University of London. 1961.
12	F. J. M. Farley	*Elements of Pulse Circuits.* Methuen. 1956.
13	D. H. Edwards	A piezo-electric pressure bar gauge. *J. Sci. Instrum.* Vol. 35. No. 9. p. 346. 1958.
14	B. D. Henshall	Shock speed and running-time measurements in the N.P.L. Hypersonic Shock Tunnel. A.R.C. C.P.443. January, 1959.

REFERENCES—*continued*

No.	*Author(s)*	*Title, etc.*
15	V. H. Blackman	Vibrational relaxation in oxygen and nitrogen. *J. Fluid Mech.* Vol. 1. Part 1. p. 61. 1956.
16	B. D. Henshall and D. L. Schultz	Some notes on the use of resistance thermometers for the measurement of heat transfer rates in shock tubes. A.R.C. C.P.408. May, 1958.
17	I. I. Glass	Theory and performance of simple shock tubes. University of Toronto, UTIA Review No. 12. Part I. 1958.
18	R. J. Emrich and C. W. Curtis ..	Attenuation in the shock tube. *J. App. Phys.* Vol. 24. No. 3. p. 360. 1953.
19	W. Chester	The propagation of shock waves in a channel of non-uniform width. *Quart. J. Mech. App. Math.* Vol. 6. Part 4. p. 440. 1953.
20	R. F. Chisnell	Motion of a shock wave in a channel with applications to cylindrical and spherical shock waves. *J. Fluid Mech.* Vol. 2. Part 3. p. 286. 1957.
21	G. F. Anderson	Shock-tube testing time. *J. Ae. Sci.* Vol. 26. No. 3. p. 184. 1959.
22	L. Bernstein	Notes on some experimental and theoretical results for the boundary layer development aft of the shock in a shock-tube. A.R.C. C.P.625. April, 1961.

TABLE 1

Range of Initial Conditions Investigated and Number of Runs Averaged in each Case

Diaphragm pressure ratio, P_{41}	100		300					2000		4000			10000	
Channel pressure, p_1 mm Hg	25	125	5	10	25	50	100	1	5	1	2	5	1	2
Circular-cross-section channel	7	4	—	—	5	—	—	—	—	6	5	4	—	6
Square-cross-section channel	4	4	4	4	4	2	4	6	4	4	4	5	5	4
Converging channel	—	5	—	—	—	—	5	—	4	—	—	—	4	—
Diverging channel	—	—	—	3	4	—	3	—	4	—	—	—	3	—

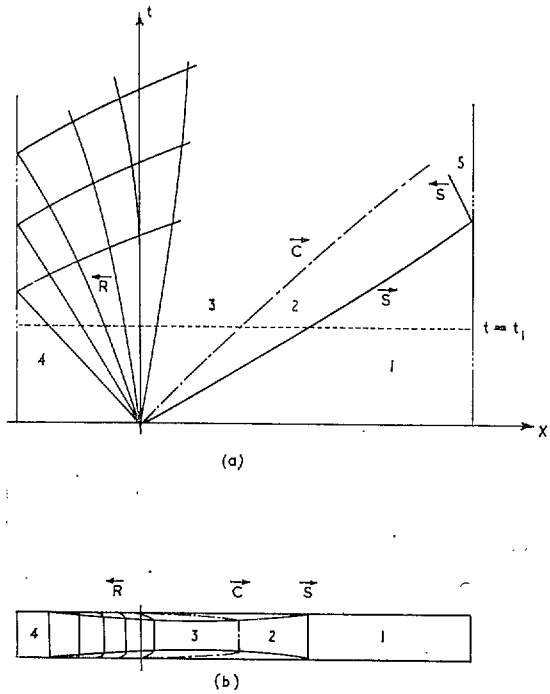

FIG. 1. Non-ideal gas flow in the shock tube.

(*a*) Distance-time plane.

(*b*) Physical plane, $t = t_1$.

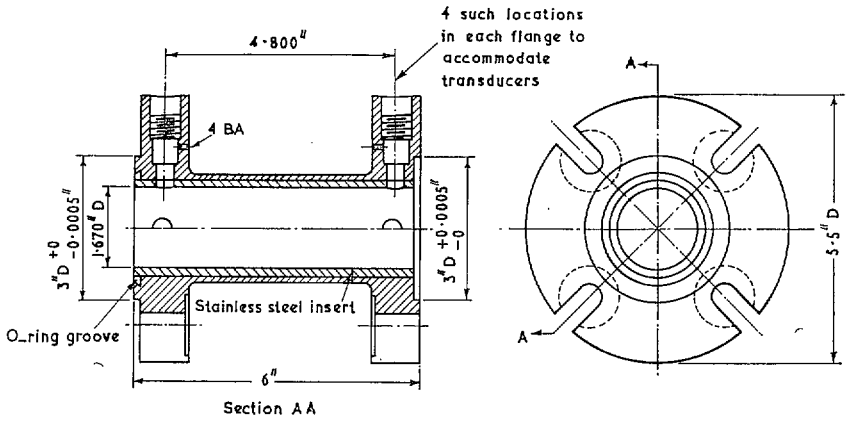

FIG. 2. The transducer-mounting sections for the circular-bore shock tube.

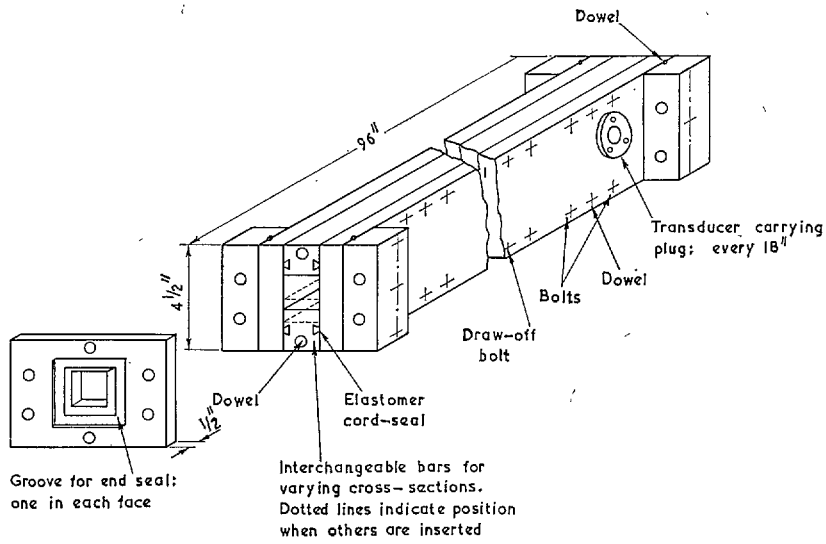

FIG. 3. The rectangular-bore shock tube, one length is shown illustrating the vacuum seals and the coupling plate.

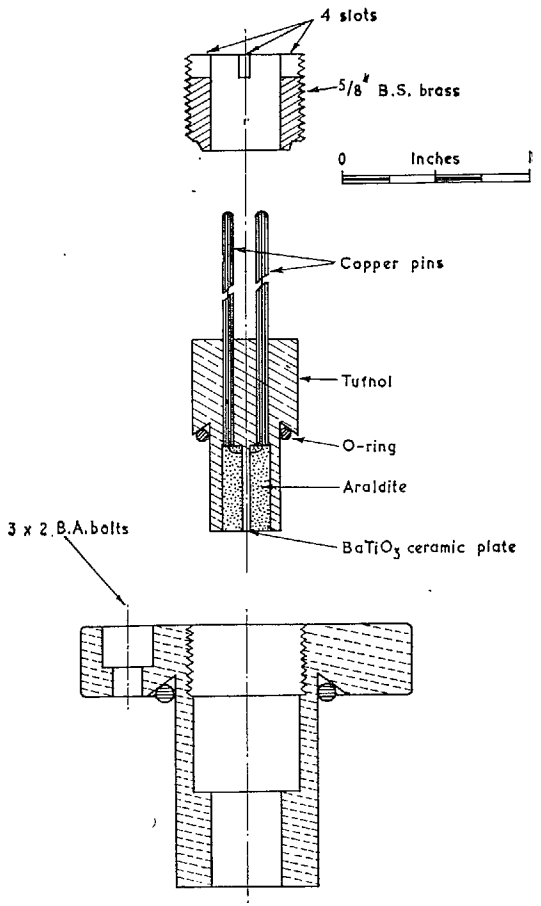

FIG. 4. Transducer and mount.

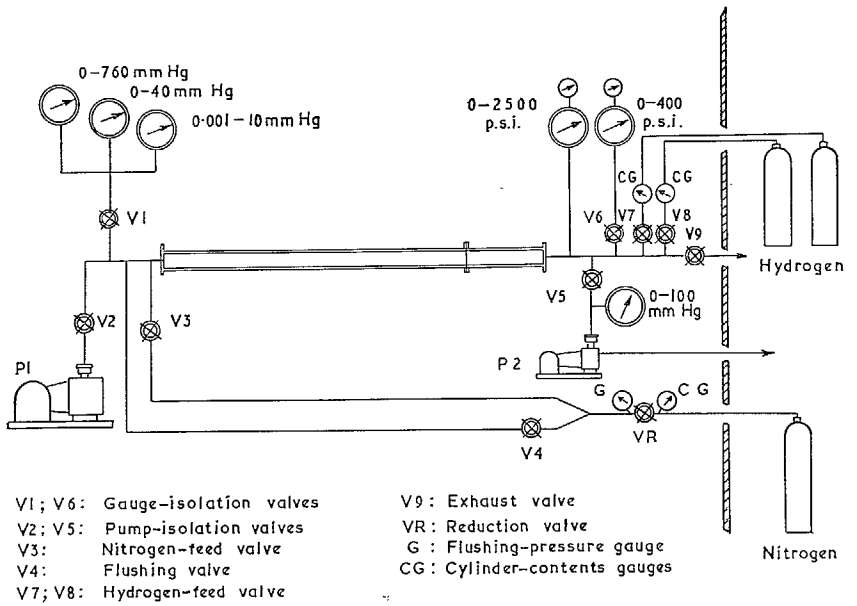

FIG. 5. Schematic diagram of gas-supply and initial-pressure measuring system.

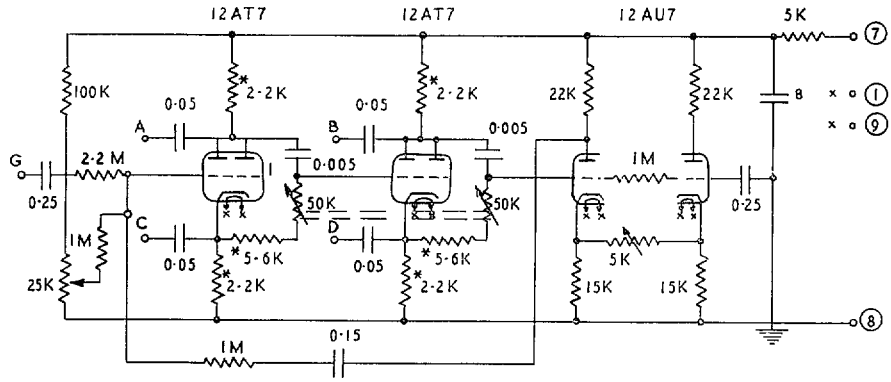

FIG. 6. Spiral-time-base generating circuit.

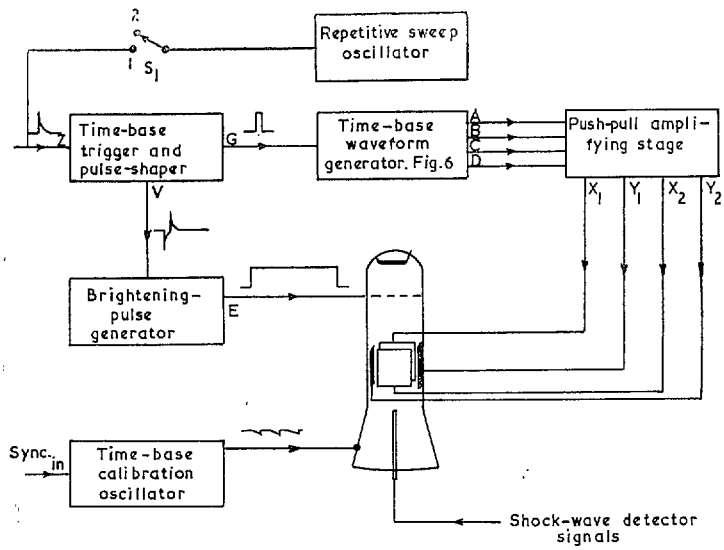

FIG. 7. Schematic diagram of high-resolution, long-duration time-base.

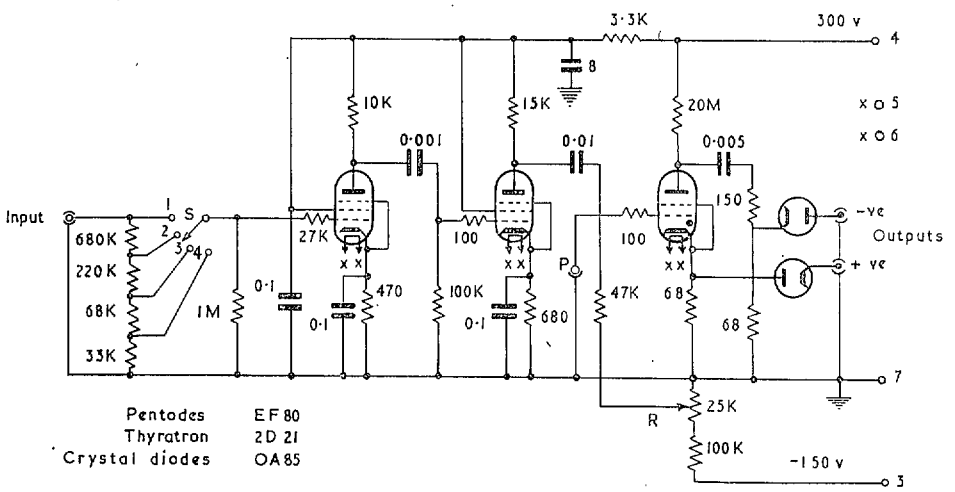

FIG. 8. Amplifier trigger unit used with barium titanate shock-wave detectors.

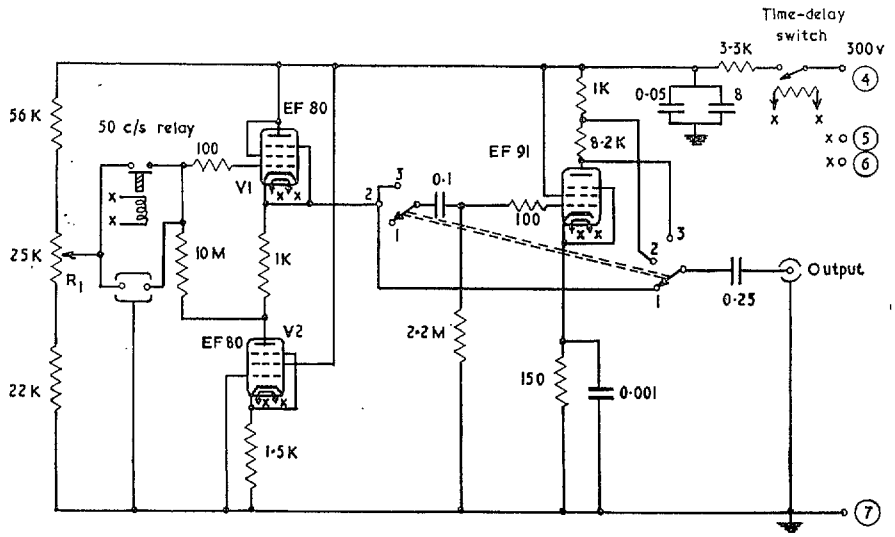

FIG. 9. Cathode-follower amplifier for pressure transducer.

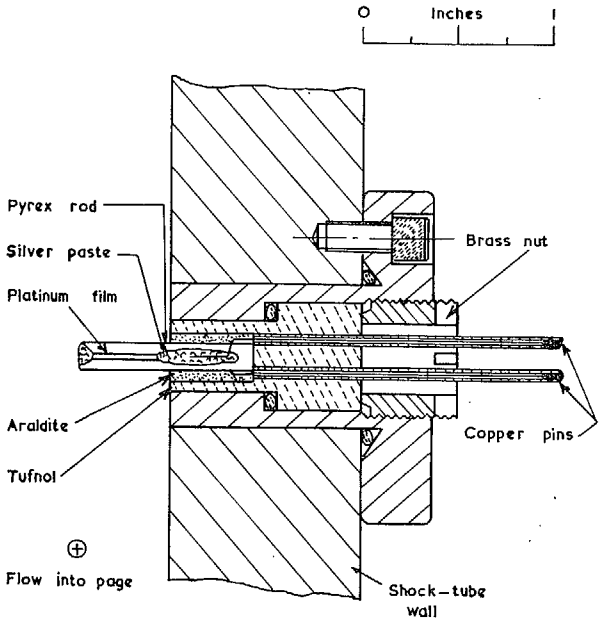

FIG. 10. Stagnation-temperature probe for interface detection.

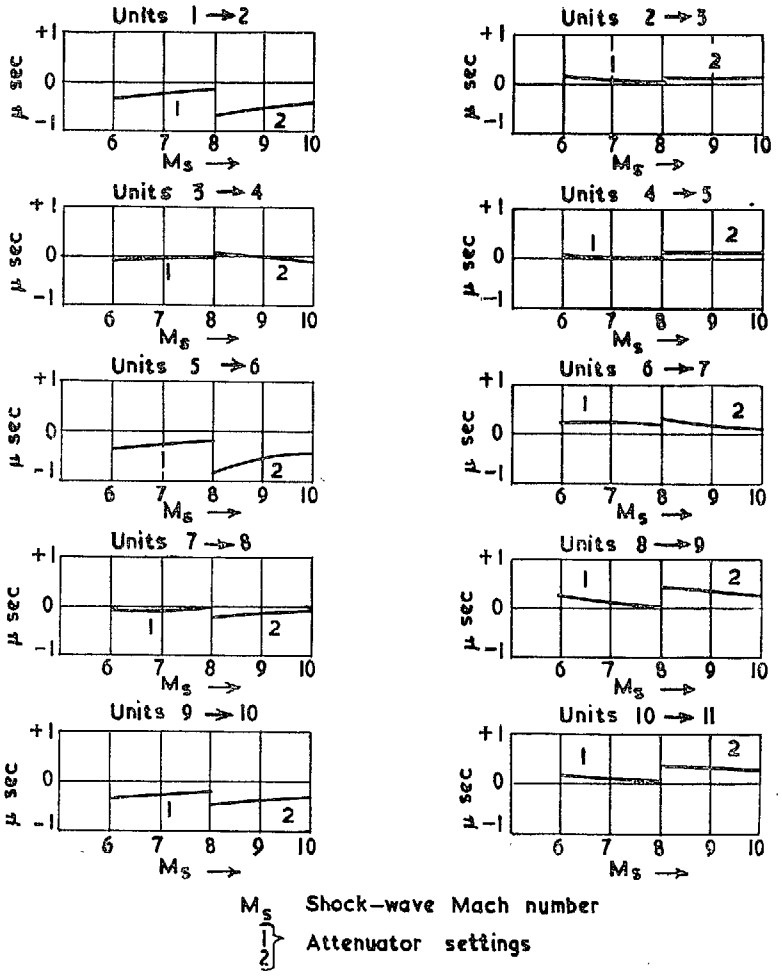

FIG. 11. Corrections to measured time intervals for a channel pressure = 2 mm Hg.

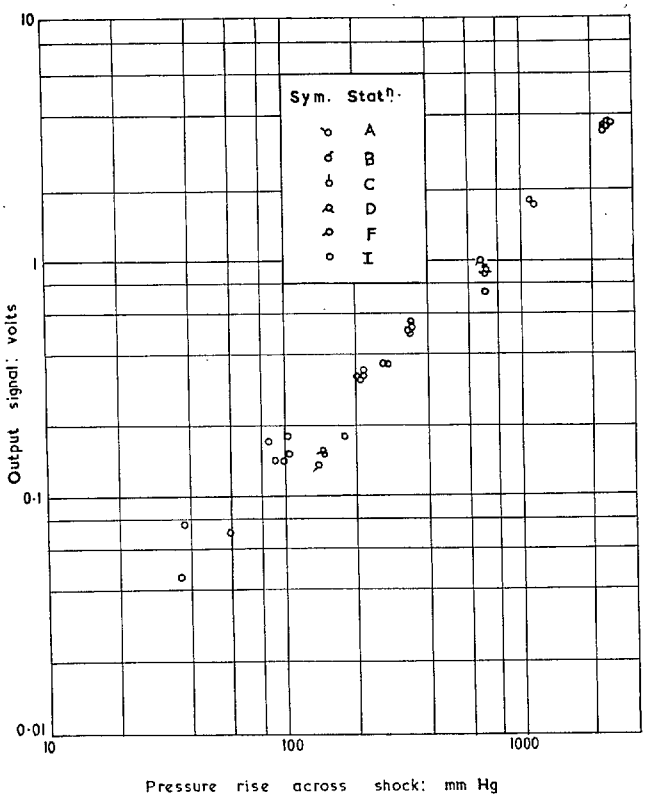

FIG. 12. Sensitivity of barium titanate ceramic transducers.

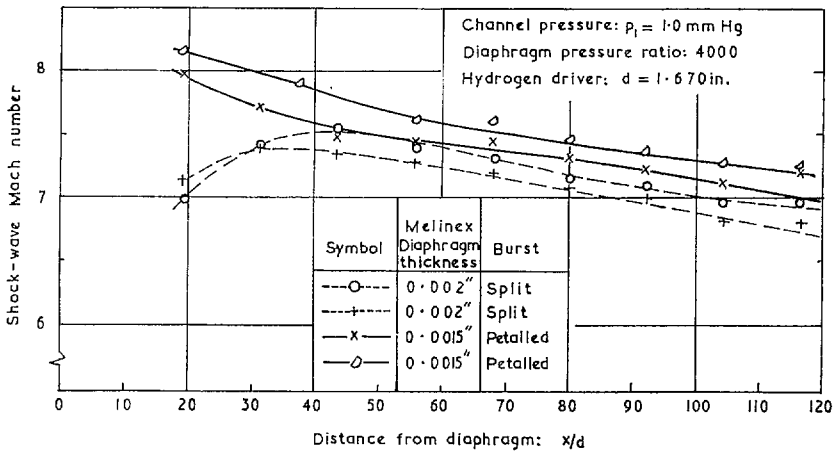

FIG. 13. Attenuation of shock waves in nitrogen. Effect of bad diaphragm burst.

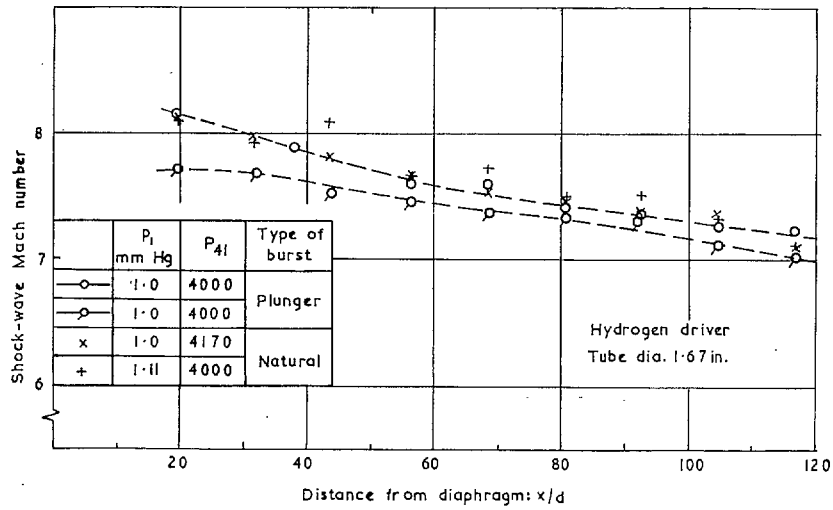

FIG. 14. Effect of diaphragm bursting method on the attenuation of shocks in nitrogen.

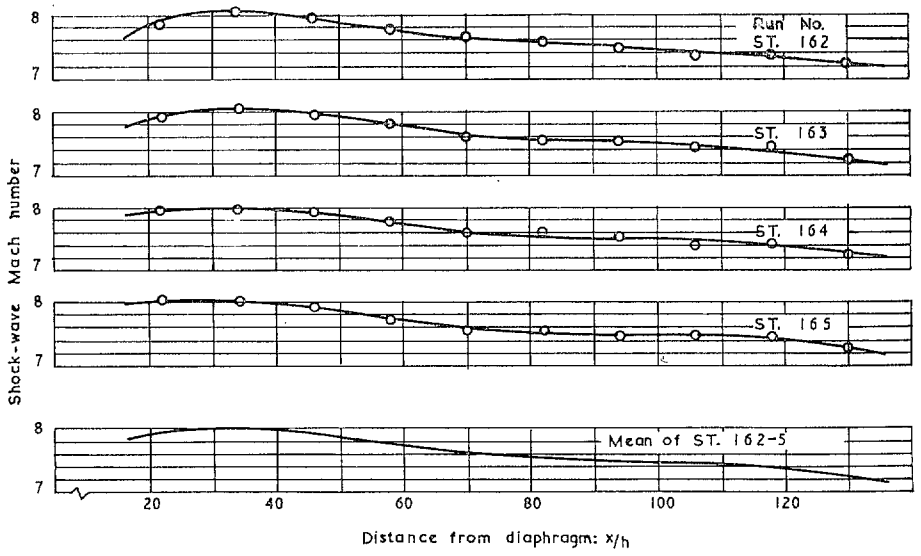

FIG. 15. Attenuation of shock waves in nitrogen. Hydrogen driver—channel pressure: 2 mm Hg.

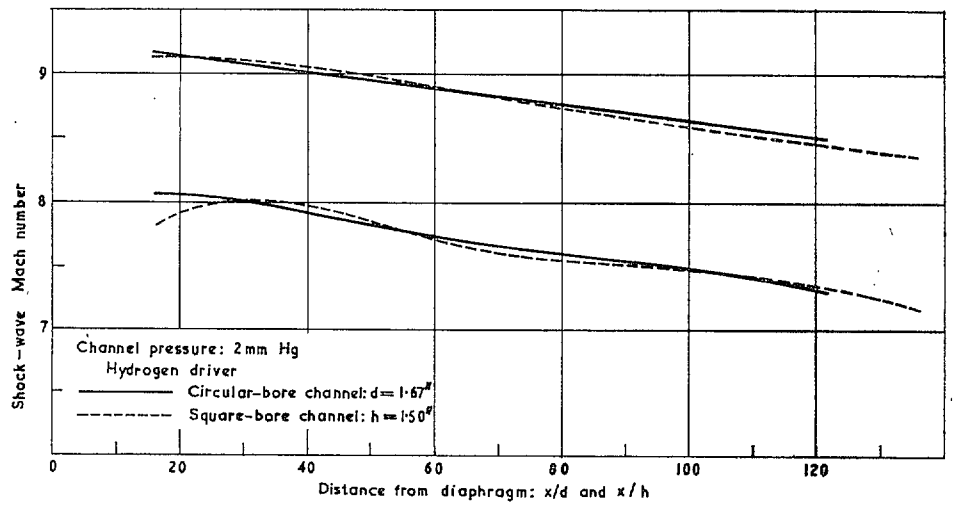

FIG. 16a. Comparison of shock attenuation in two channels.

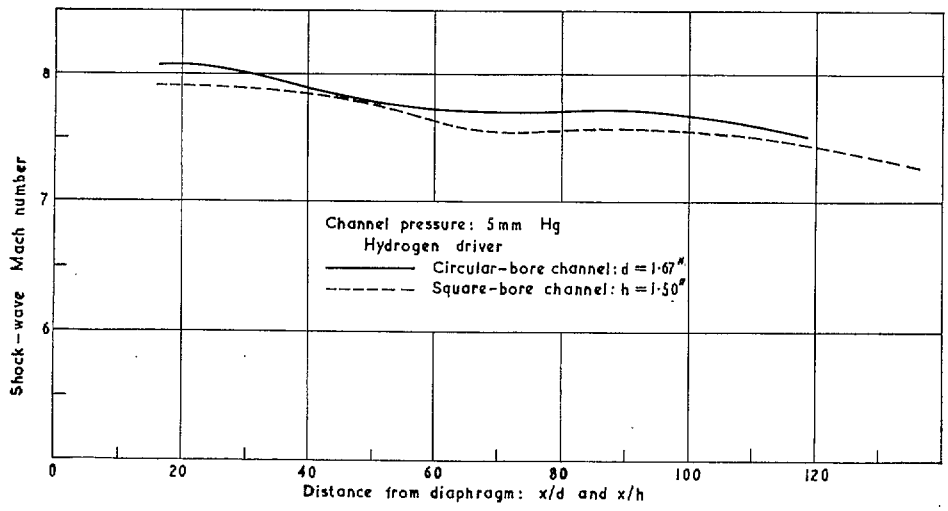

FIG. 16b. Comparison of shock attenuation in two channels.

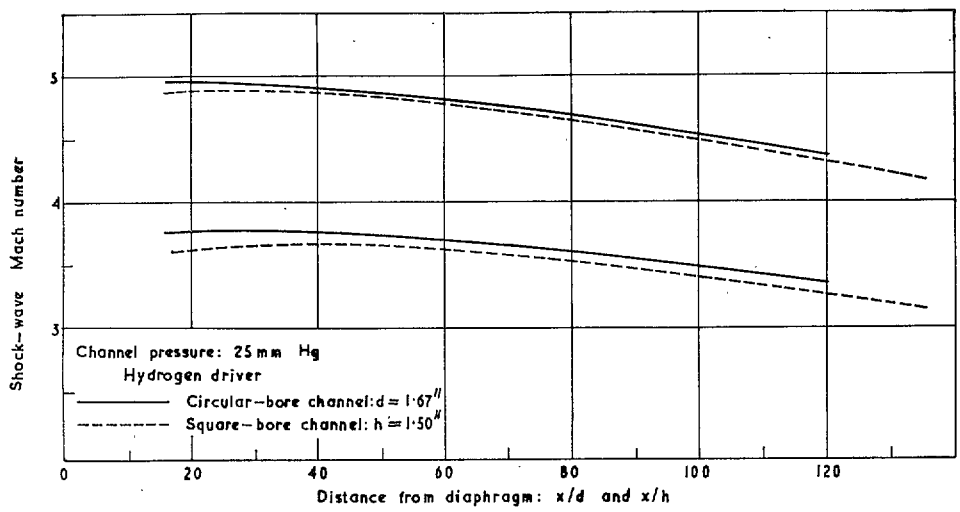

FIG. 16c. Comparison of shock attenuation in two channels.

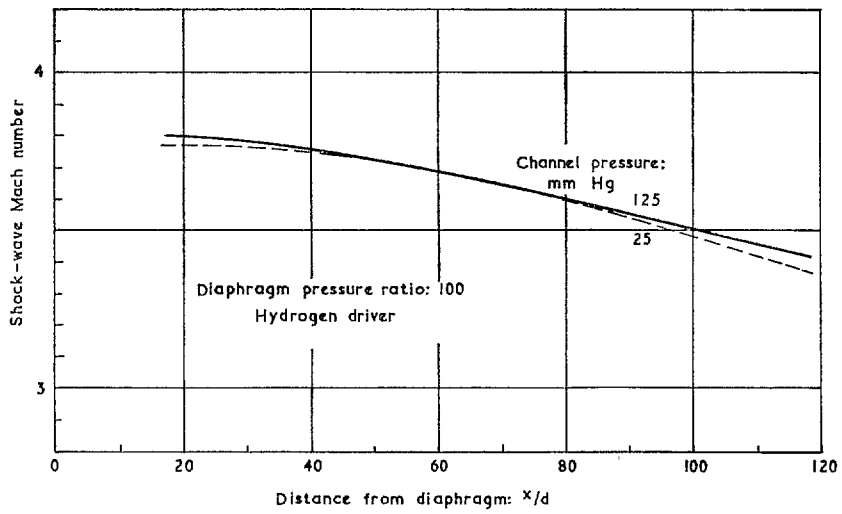

FIG. 17a. Attenuation of shocks in nitrogen. Effect of channel pressure.

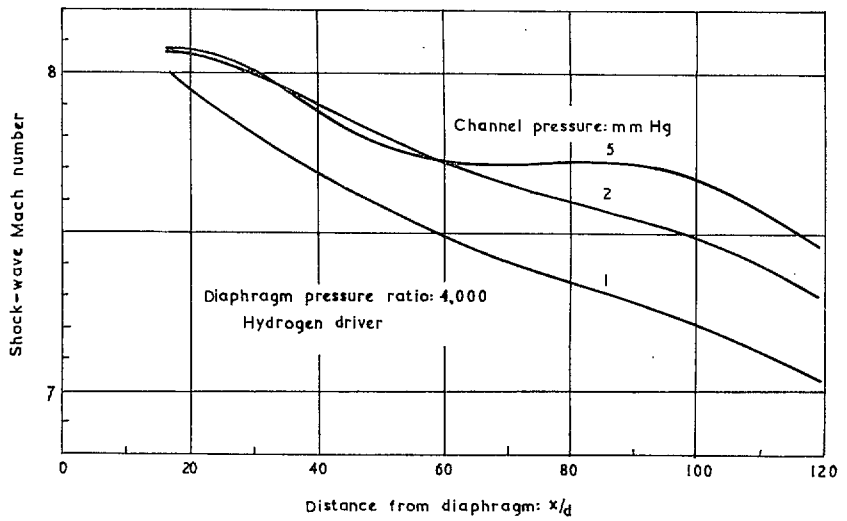

FIG. 17b. Attenuation of shocks in nitrogen. Effect of channel pressure.

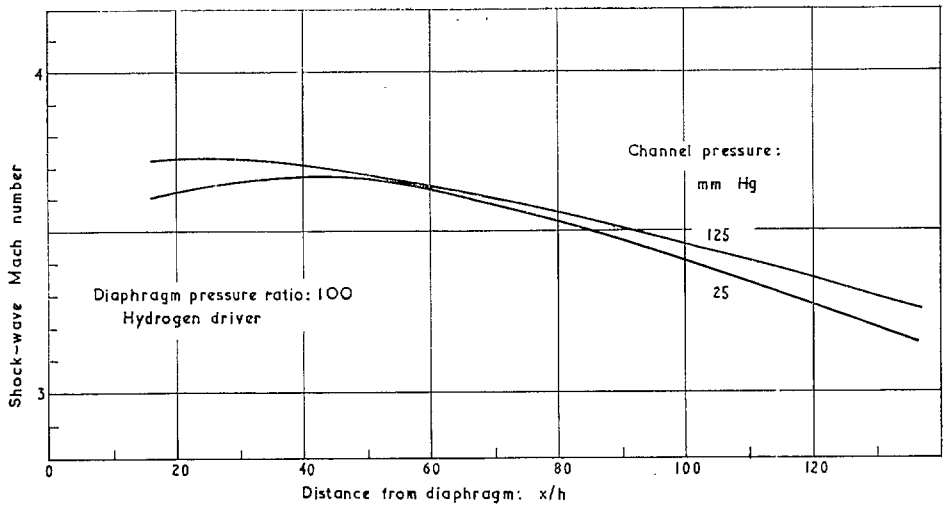

FIG. 18a. Attenuation of shocks in nitrogen. Effect of channel pressure.

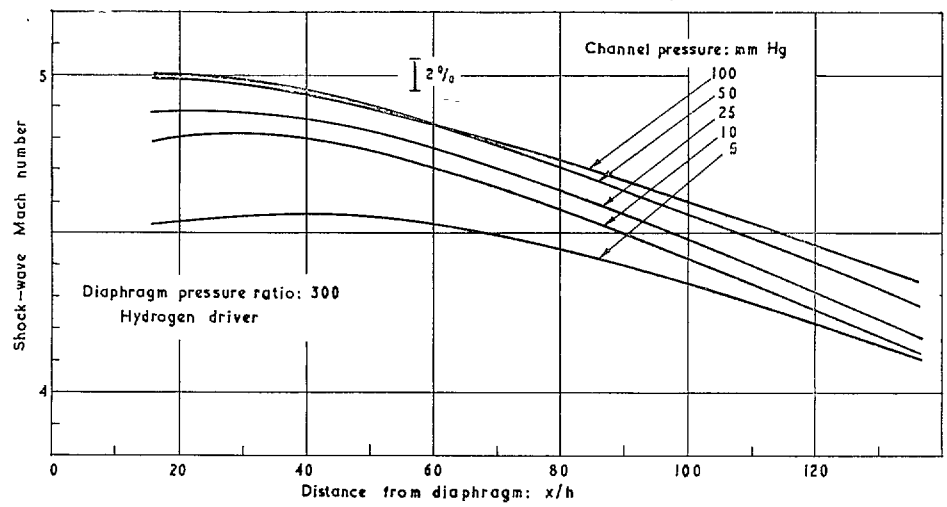

FIG. 18b. Attenuation of shocks in nitrogen. Effect of channel pressure.

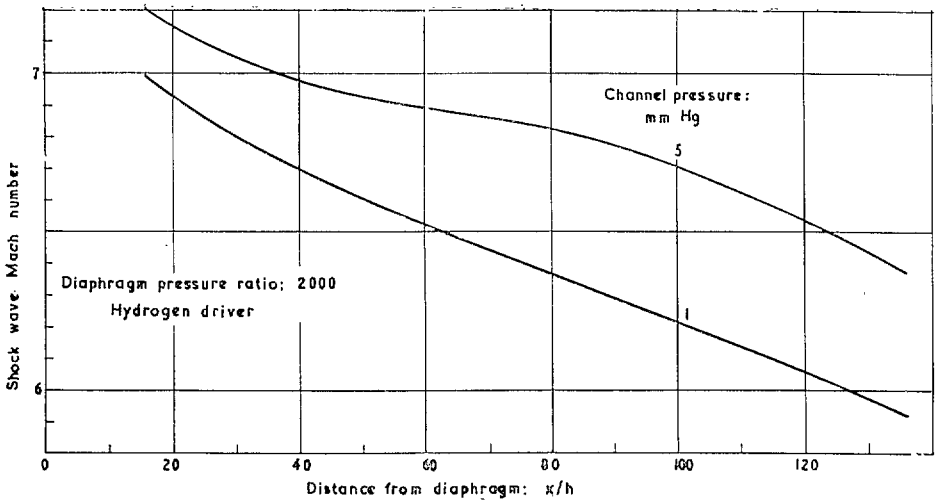

FIG. 18c. Attenuation of shocks in nitrogen. Effect of channel pressure.

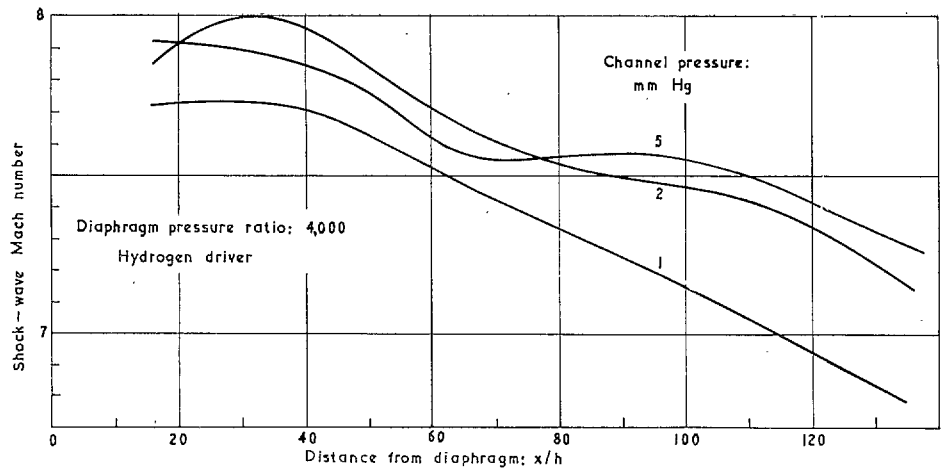

FIG. 18d. Attenuation of shocks in nitrogen. Effect of channel pressure.

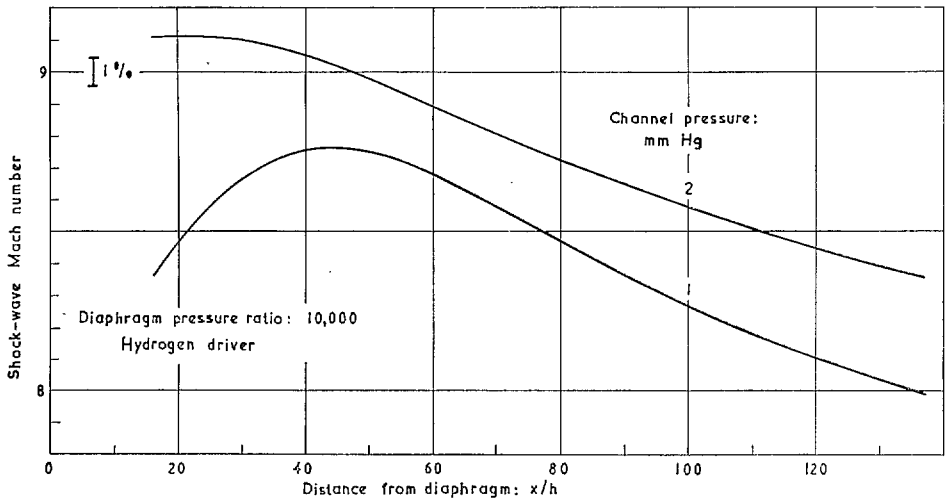

FIG. 18e. Attenuation of shocks in nitrogen. Effect of channel pressure.

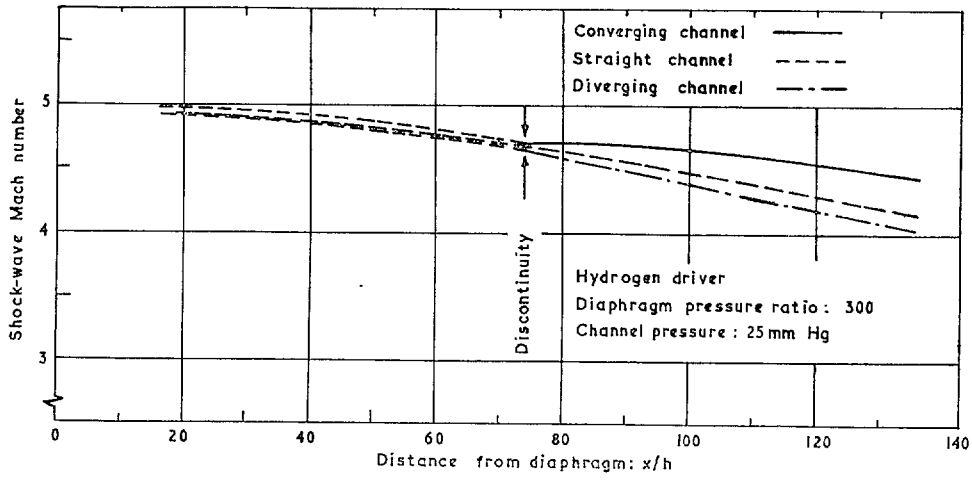

FIG. 19a. Comparison of shock attenuation in variable-bore channels: nitrogen.

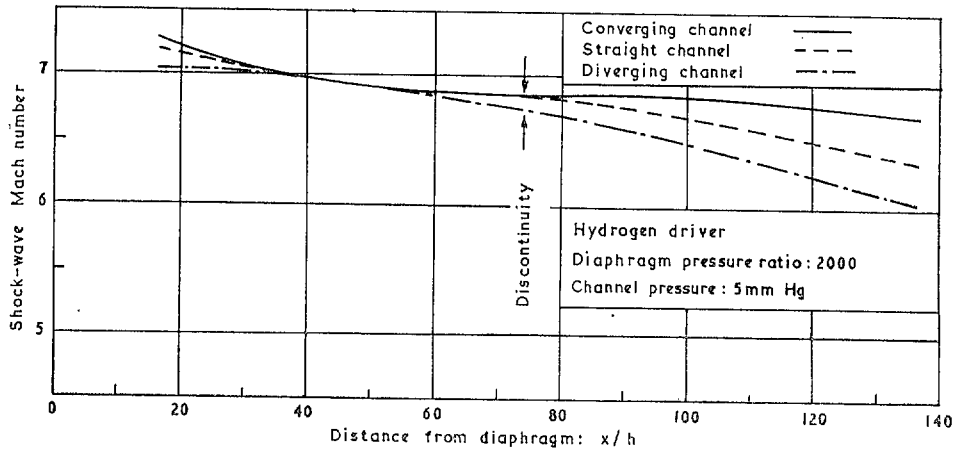

FIG. 19b. Comparison of shock attenuation in variable-bore channels: nitrogen.

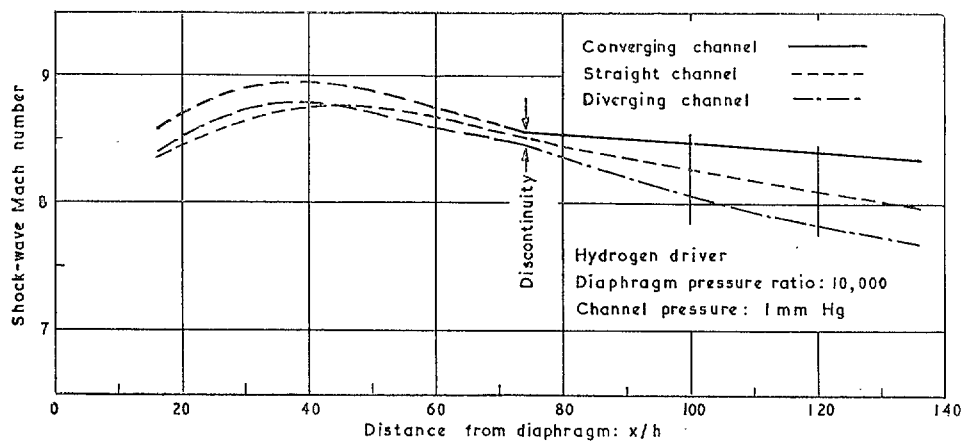

FIG. 19c. Comparison of shock attenuation in variable-bore channels: nitrogen.

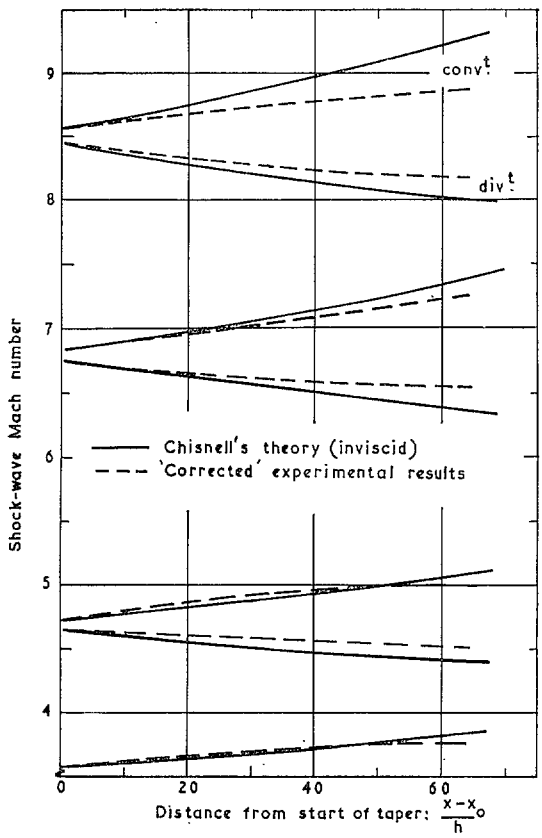

FIG. 20. Shock trajectories in variable-bore tubes.

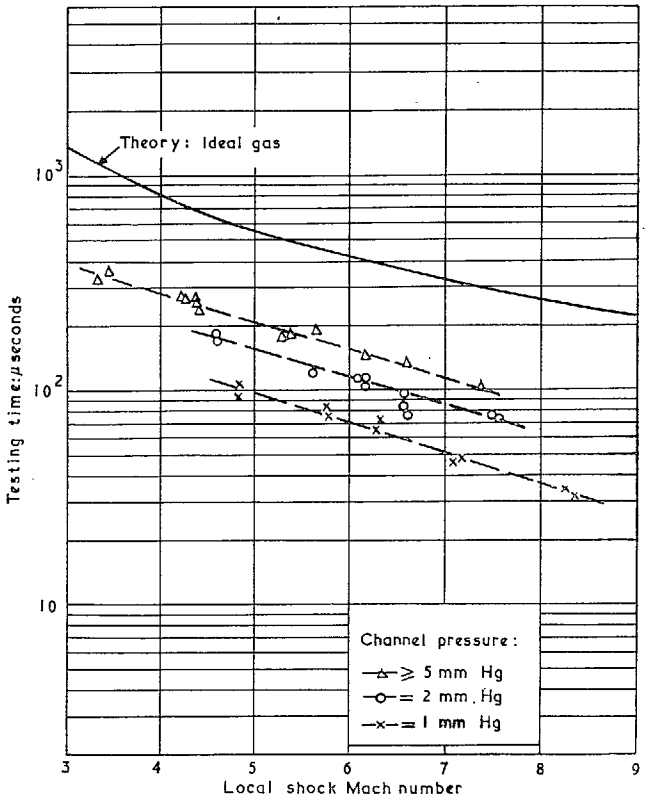

FIG. 21. Testing time at station 14 ft from diaphragm: straight tube.

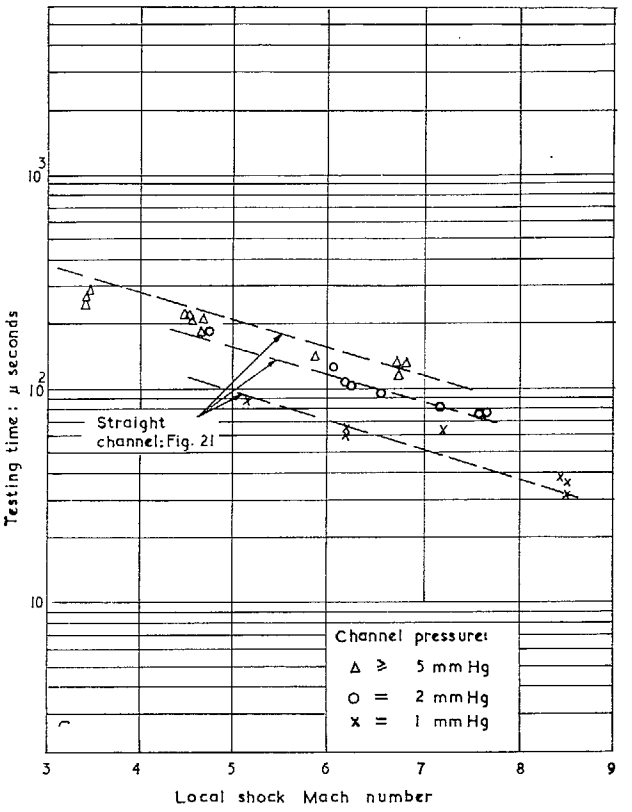

FIG. 22. Testing time at station 14 ft from diaphragm: converging channel.

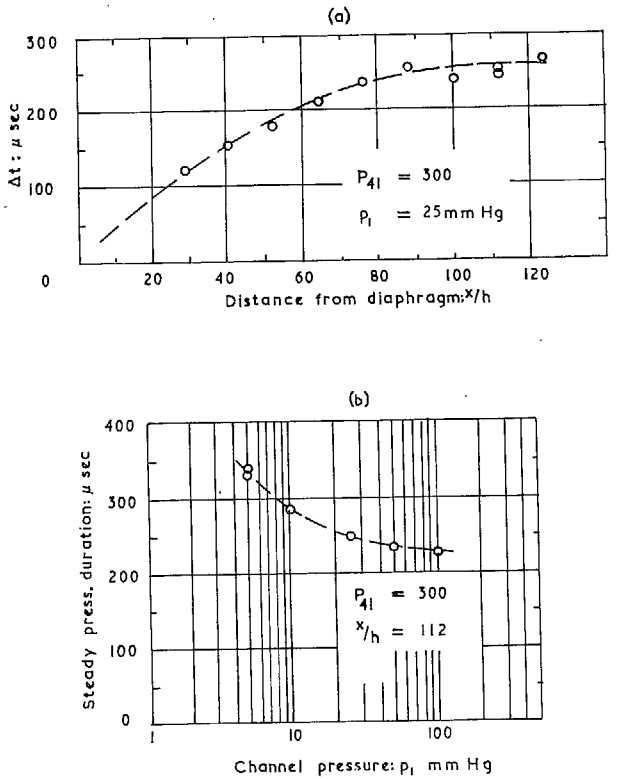

FIG. 23. Steady-pressure duration behind shock at constant diaphragm pressure ratio.

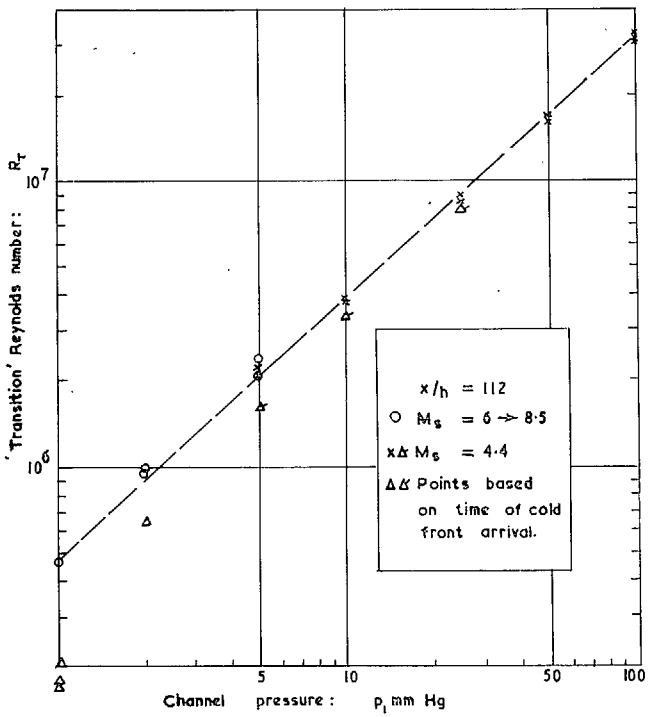

FIG. 24. 'Transition' Reynolds number: $R_T = \rho_2 u_2 w_1 (\Gamma_{21} - 1)\Delta t/\mu_2$.

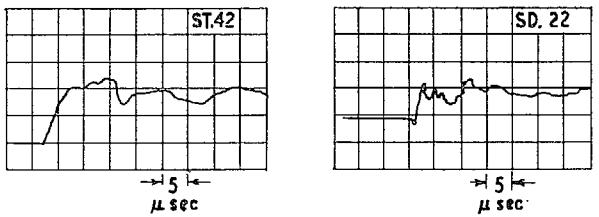

(a) (b)

Transducer response time: Plate size; (a) 1/2" x 1/4" x 0·02" (b) 1/8" x 1/8" x 0·02"

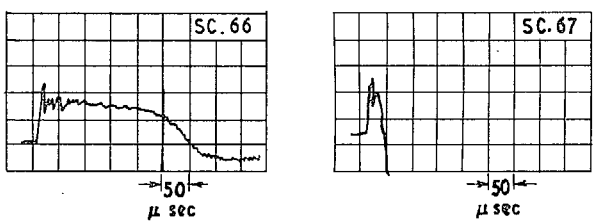

(c) (d)

Transducer not insulated from flow: (c) Shock Mach number = 4·47 (d) Shock Mach number = 6·83

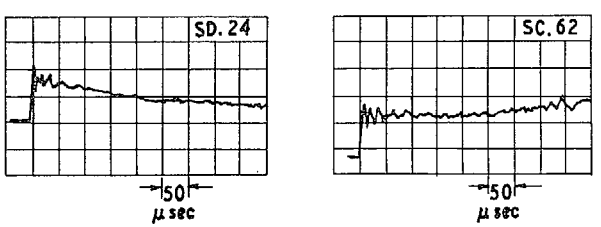

(e) (f)

Transducer insulated from flow (e) Connected directly to C.R.O. (f) Connected via cathode-follower amplifier

PLATE I. Typical piezoelectric transducer responses.

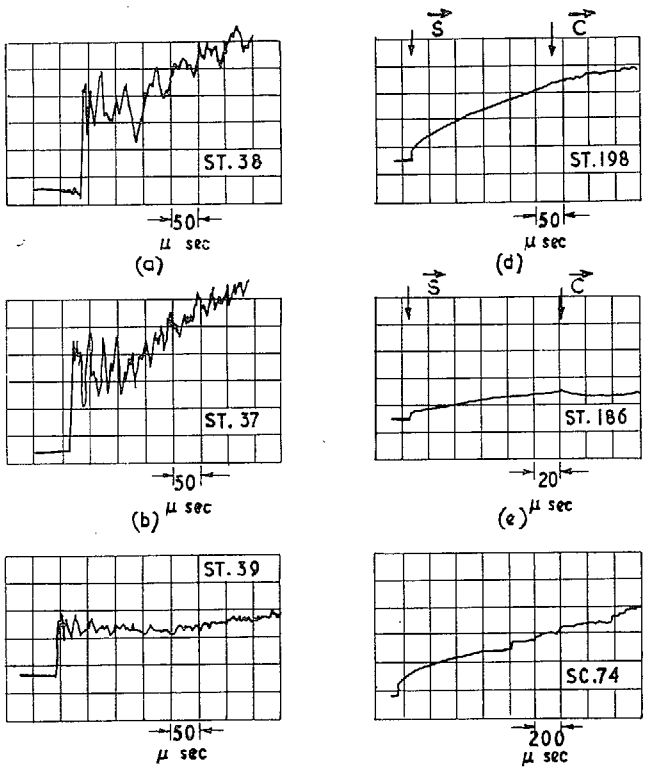

$BaTiO_3$, transducer responses:
(a) Showing pickup of mechanical vibration before shock arrival,
(b) Showing elimination of pre-shock vibration - W_{11} = 7·66; p_1 = 2mm Hg,
(c) As (b) but with W_{11} = 4·81 and p_1 = 25mm Hg

Stagnation thermometer responses:
(d) Shock Mach number = 4·36
(e) Shock Mach number = 6·12
(f) Shock Mach number = 2·13 showing secondary waves in converging channel.

PLATE II. Piezoelectric and thin-film-thermometer signals.

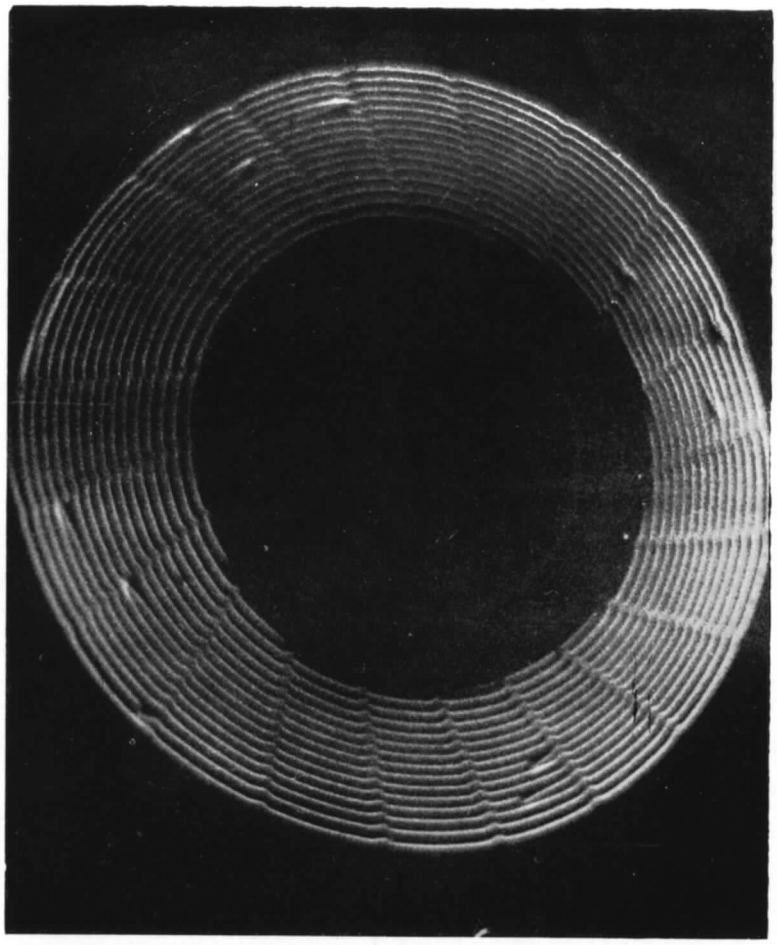

PLATE III. A typical C.R.O. spiral time-base: 100 kc/s marker frequency.

(87121) Wt. 64/1857 K.5 7/63 Hw.

Publications of the Aeronautical Research Council

ANNUAL TECHNICAL REPORTS OF THE AERONAUTICAL RESEARCH COUNCIL (BOUND VOLUMES)

1942 Vol. I. Aero and Hydrodynamics, Aerofoils, Airscrews, Engines. 75*s.* (post 2*s.* 9*d.*)
Vol. II. Noise, Parachutes, Stability and Control, Structures, Vibration, Wind Tunnels. 47*s.* 6*d.* (post 2*s.* 3*d.*)

1943 Vol. I. Aerodynamics, Aerofoils, Airscrews. 80*s.* (post 2*s.* 6*d.*)
Vol. II. Engines, Flutter, Materials, Parachutes, Performance, Stability and Control, Structures. 90*s.* (post 2*s.* 9*d.*)

1944 Vol. I. Aero and Hydrodynamics, Aerofoils, Aircraft, Airscrews, Controls. 84*s.* (post 3*s.*)
Vol. II. Flutter and Vibration, Materials, Miscellaneous, Navigation, Parachutes, Performance, Plates and Panels, Stability, Structures, Test Equipment, Wind Tunnels. 84*s.* (post 3*s.*)

1945 Vol. I. Aero and Hydrodynamics, Aerofoils. 130*s.* (post 3*s.* 6*d.*)
Vol. II. Aircraft, Airscrews, Controls. 130*s.* (post 3*s.* 6*d.*)
Vol. III. Flutter and Vibration, Instruments, Miscellaneous, Parachutes, Plates and Panels, Propulsion. 130*s.* (post 3*s.* 3*d.*)
Vol. IV. Stability, Structures, Wind Tunnels, Wind Tunnel Technique. 130*s.* (post 3*s.* 3*d.*)

1946 Vol. I. Accidents, Aerodynamics, Aerofoils and Hydrofoils. 168*s.* (post 3*s.* 9*d.*)
Vol. II. Airscrews, Cabin Cooling, Chemical Hazards, Controls, Flames, Flutter, Helicopters, Instruments and Instrumentation, Interference, Jets, Miscellaneous, Parachutes. 168*s.* (post 3*s.* 3*d.*)
Vol. III. Performance, Propulsion, Seaplanes, Stability, Structures, Wind Tunnels. 168*s.* (post 3*s.* 6*d.*)

1947 Vol. I. Aerodynamics, Aerofoils, Aircraft. 168*s.* (post 3*s.* 9*d.*)
Vol. II. Airscrews and Rotors, Controls, Flutter, Materials, Miscellaneous, Parachutes, Propulsion, Seaplanes, Stability, Structures, Take-off and Landing. 168*s.* (post 3*s.* 9*d.*)

1948 Vol. I. Aerodynamics, Aerofoils, Aircraft, Airscrews, Controls, Flutter and Vibration, Helicopters, Instruments, Propulsion, Seaplane, Stability, Structures, Wind Tunnels. 130*s.* (post 3*s.* 3*d.*)
Vol. II. Aerodynamics, Aerofoils, Aircraft, Airscrews, Controls, Flutter and Vibration, Helicopters, Instruments, Propulsion, Seaplane, Stability, Structures, Wind Tunnels. 110*s.* (post 3*s.* 3*d.*)

Special Volumes

Vol. I. Aero and Hydrodynamics, Aerofoils, Controls, Flutter, Kites, Parachutes, Performance, Propulsion, Stability. 126*s.* (post 3*s.*)
Vol. II. Aero and Hydrodynamics, Aerofoils, Airscrews, Controls, Flutter, Materials, Miscellaneous, Parachutes, Propulsion, Stability, Structures. 147*s.* (post 3*s.*)
Vol. III. Aero and Hydrodynamics, Aerofoils, Airscrews, Controls, Flutter, Kites, Miscellaneous, Parachutes, Propulsion, Seaplanes, Stability, Structures, Test Equipment. 189*s.* (post 3*s.* 9*d.*)

Reviews of the Aeronautical Research Council

1939–48 3*s.* (post 6*d.*) 1949–54 5*s.* (post 5*d.*)

Index to all Reports and Memoranda published in the Annual Technical Reports

1909–1947 R. & M. 2600 (out of print)

Indexes to the Reports and Memoranda of the Aeronautical Research Council

Between Nos. 2351–2449	R. & M. No. 2450	2*s.* (post 3*d.*)
Between Nos. 2451–2549	R. & M. No. 2550	2*s.* 6*d.* (post 3*d.*)
Between Nos. 2551–2649	R. & M. No. 2650	2*s.* 6*d.* (post 3*d.*)
Between Nos. 2651–2749	R. & M. No. 2750	2*s.* 6*d.* (post 3*d.*)
Between Nos. 2751–2849	R. & M. No. 2850	2*s.* 6*d.* (post 3*d.*)
Between Nos. 2851–2949	R. & M. No. 2950	3*s.* (post 3*d.*)
Between Nos. 2951–3049	R. & M. No. 3050	3*s.* 6*d.* (post 3*d.*)
Between Nos. 3051–3149	R. & M. No. 3150	3*s.* 6*d.* (post 3*d.*)

HER MAJESTY'S STATIONERY OFFICE

from the addresses overleaf

Printed and published by
HER MAJESTY'S STATIONERY OFFICE

To be purchased from
York House, Kingsway, London W.C.2
423 Oxford Street, London W.1
13A Castle Street, Edinburgh 2
109 St. Mary Street, Cardiff
39 King Street, Manchester 2
50 Fairfax Street, Bristol 1
35 Smallbrook, Ringway, Birmingham 5
80 Chichester Street, Belfast 1
or through any bookseller

Printed in England

S.O. Code No. 23-3321